

GENERAL ARTICLE

The phenotypic landscape of a *Tbc1d24* mutant mouse includes convulsive seizures resembling human early infantile epileptic encephalopathy

Risa Tona^{1,2}, Wenqian Chen¹, Yoko Nakano³, Laura D. Reyes⁴, Ronald S. Petralia⁵, Ya-Xian Wang⁵, Matthew F. Starost⁶, Talah T. Wafa⁷, Robert J. Morell⁸, Kevin D. Cravedi⁹, Johann du Hoffmann⁹, Takushi Miyoshi¹, Jeeva P. Munasinghe¹⁰, Tracy S. Fitzgerald⁷, Yogita Chudasama^{9,11}, Koichi Omori², Carlo Pierpaoli⁴, Botond Banfi³, Lijin Dong¹², Inna A. Belyantseva¹ and Thomas B. Friedman^{1,*†}

¹Laboratory of Molecular Genetics, National Institute on Deafness and Other Communication Disorders, Porter Neuroscience Research Center, National Institutes of Health, Bethesda, MD 20892, USA, ²Department of Otolaryngology, Head and Neck Surgery, Graduate School of Medicine, Kyoto University, 606-8507 Kyoto, Japan, ³Department of Anatomy and Cell Biology, Carver College of Medicine, University of Iowa, Iowa City, IA 52242, USA, ⁴Quantitative Medical Imaging Section, National Institute of Biomedical Imaging and Bioengineering, National Institutes of Health, Bethesda, MD 20892, USA, ⁵Advanced Imaging Core, National Institute on Deafness and Other Communication Disorders, National Institutes of Health, Bethesda, MD 20892, USA, ⁶Division of Veterinary Resources, National Institutes of Health, Bethesda, MD 20892, USA, ⁷Mouse Auditory Testing Core Facility, National Institute on Deafness and Other Communication Disorders, National Institutes of Health, Bethesda, MD 20892, USA, ⁸Genomics and Computational Biology Core, National Institute on Deafness and Other Communication Disorders, National Institutes of Health, Bethesda, MD 20892, USA, ⁹Rodent Behavioral Core, National Institute of Mental Health, Porter Neuroscience Research Center, National Institutes of Health, Bethesda, MD 20892, USA, ¹⁰Mouse Imaging Facility, *In vivo* NMR Center, National Institute of Neurological Disorders and Stroke, National Institutes of Health, Bethesda, MD 20892, USA, ¹¹Section on Behavioral Neuroscience, National Institute of Mental Health, Porter Neuroscience Research Center, National Institutes of Health, Bethesda, MD 20892, USA and ¹²Genetic Engineering Core, National Eye Institute, National Institutes of Health, Bethesda, MD 20892, USA

*To whom correspondence should be addressed at: National Institute on Deafness and Other Communication Disorders, Porter Neuroscience Research Center, Room 1F141, National Institutes of Health, Bethesda, MD 20892, USA. Tel: +301 4967882; Fax: +301 4024200; Email: friedman@nidcd.nih.gov

†Thomas B. Friedman, <http://orcid.org/0000-0003-4614-6630>

Received: October 28, 2018. Revised: December 2, 2018. Accepted: December 11, 2018

Published by Oxford University Press 2019.

This work is written by US Government employees and is in the public domain in the US.

Abstract

Epilepsy, deafness, onychodystrophy, osteodystrophy and intellectual disability are associated with a spectrum of mutations of human *TBC1D24*. The mechanisms underlying *TBC1D24*-associated disorders and the functions of *TBC1D24* are not well understood. Using CRISPR-Cas9 genome editing, we engineered a mouse with a premature translation stop codon equivalent to human S324Tfs*3, a recessive mutation of *TBC1D24* associated with early infantile epileptic encephalopathy (EIEE). Homozygous S324Tfs*3 mice have normal auditory and vestibular functions but show an abrupt onset of spontaneous seizures at postnatal day 15 recapitulating human EIEE. The S324Tfs*3 variant is located in an alternatively spliced micro-exon encoding six perfectly conserved amino acids incorporated postnatally into *TBC1D24* protein due to a micro-exon utilization switch. During embryonic and early postnatal development, S324Tfs*3 homozygotes produce predominantly the shorter wild-type *TBC1D24* protein isoform that omits the micro-exon. S324Tfs*3 homozygotes show an abrupt onset of seizures at P15 that correlates with a developmental switch to utilization of the micro-exon. A mouse deficient for alternative splice factor SRRM3 impairs incorporation of the *Tbc1d24* micro-exon. Wild-type *Tbc1d24* mRNA is abundantly expressed in the hippocampus using RNAscope *in situ* hybridization. Immunogold electron microscopy using a *TBC1D24*-specific antibody revealed that *TBC1D24* is associated with clathrin-coated vesicles and synapses of hippocampal neurons, suggesting a crucial role of *TBC1D24* in vesicle trafficking important for neuronal signal transmission. This is the first characterization of a mouse model of human *TBC1D24*-associated EIEE that can now be used to screen for antiepileptogenic drugs ameliorating *TBC1D24* seizure disorders.

Introduction

The human genome encodes 42 proteins that contain TBC domains (Tre-2-Bub2-Cdc16) (1), an ancient, conserved sequence consisting of approximately 200 amino acids (2). Pathogenic variants of several genes encoding TBC domains contribute to a range of disorders in humans, including epilepsy, intellectual disability, pontocerebellar hypoplasia, dysmorphic features and deafness (Table 1) (3–7). Studies of these disorders have contributed to an appreciation of the broad range of *in vivo* functions of TBC-containing proteins, although their pathophysiology is not fully understood. Surprisingly, different pathogenic mutations of human *TBC1D24* (TBC1 domain family member 24, OMIM 613577; Fig. 1A) are associated with several distinct clinical phenotypes (Table 1), including non-syndromic deafness segregating as a recessive (referred to as DFNB86 deafness) or dominant trait (DFNA65) (5,8,9), early infantile epileptic encephalopathy 16 (EIEE16) with or without deafness (10), progressive myoclonic epilepsy (PME) (11), familial infantile myoclonic epilepsy (FIME) (10) and deafness, onychodystrophy, osteodystrophy, mental retardation and seizures (DOORS) syndrome. DOORS is a multisystem disorder characterized by deafness, onychodystrophy, osteodystrophy, intellectual disability and seizures (3). Eight heterozygous *de novo* microdeletions that include *TBC1D24*, *ATP6V0C* and *PDPK1*, three closely linked genes on chromosome 16p12.3, in eight patients were associated with epilepsy and variable magnitudes of delayed development, intellectual disability and microcephaly (12).

The human *TBC1D24* gene encodes several alternatively spliced transcripts (5). The longest transcript of *TBC1D24* encodes an N-terminal TBC domain followed by 82 residues that link to a C-terminus TLDC domain (TBC, LysM and domain catalytic; Fig. 1A). This combination of TBC and TLDC domains is unique in the mammalian proteome. While some TLDC domain-containing proteins, such as OXR1 (oxidative resistance 1), have a neuro-protective role against oxidative stress (13), the function of the TLDC domain of *TBC1D24* is unknown.

Some TBC domain-containing proteins have well-established roles as GAPs (GTPase-activating protein), which inactivate RABs, an observation revealed first in studies of yeast (14).

RABs regulate protein and lipid transport between cellular compartments as well as a variety of other functions such as the biogenesis of organelles (15). However, *TBC1D24* is unlikely to be a RAB-GAP as it lacks critical RQ (arginine, glutamine) finger residues that are important for GTP hydrolysis (6,16,17). Thus, the biochemical role and cellular functions of *TBC1D24* are only partially characterized.

Following the first report of a mutation of *TBC1D24* associated with epilepsy (4,10), 55 additional pathological variants of *TBC1D24* have been reported. The phenotype associated with each variant and their locations relative to the two protein domains of *TBC1D24* are shown in Figure 1A. Presently, there is no settled association of a specific phenotype with either the location of the variant within the gene or with the variant type (missense, splice-site or truncating mutation) (18). Mutations of *TBC1D24* associated with each of the three different clinically distinctive phenotypes do not cluster in one or the other of the two domains of *TBC1D24* but rather are distributed across the primary amino acid sequence (Fig. 1A). To explain the spectrum of *TBC1D24*-associated disorders, it has been suggested that the pathogenic variants of *TBC1D24* may damage different binding motifs for its protein partners resulting in different phenotypes (6), may affect one or more alternative transcripts encoding different *TBC1D24* protein isoforms (5) or both. In addition, modifiers in the genetic background of an affected individual may influence the penetrance, severity or scope of a *TBC1D24*-associated disorder (19,20).

Insight into the functions of *TBC1D24* can be gained by a combination of observations including its expression profiles in specific cell types, localization within intracellular compartments and the composition and complexity of its protein interaction network (6,21). ARF6 (ADP-ribosylation factor) is a small GTPase crucial for membrane trafficking (10,22) that binds *TBC1D24*, which may modulate ARF6 activation that regulates vesicle trafficking (10,22). In *Xenopus laevis*, *TBC1D24* interacts indirectly with ephrinB2 through Dishevelled and is important for cranial neural crest migration (23). Additionally, mutations of Sky, the *Drosophila melanogaster* ortholog of mammalian *TBC1D24*, result in severe brain lesions and seizure-like behavior due to deficits of presynaptic trafficking of vesicles (2,17).

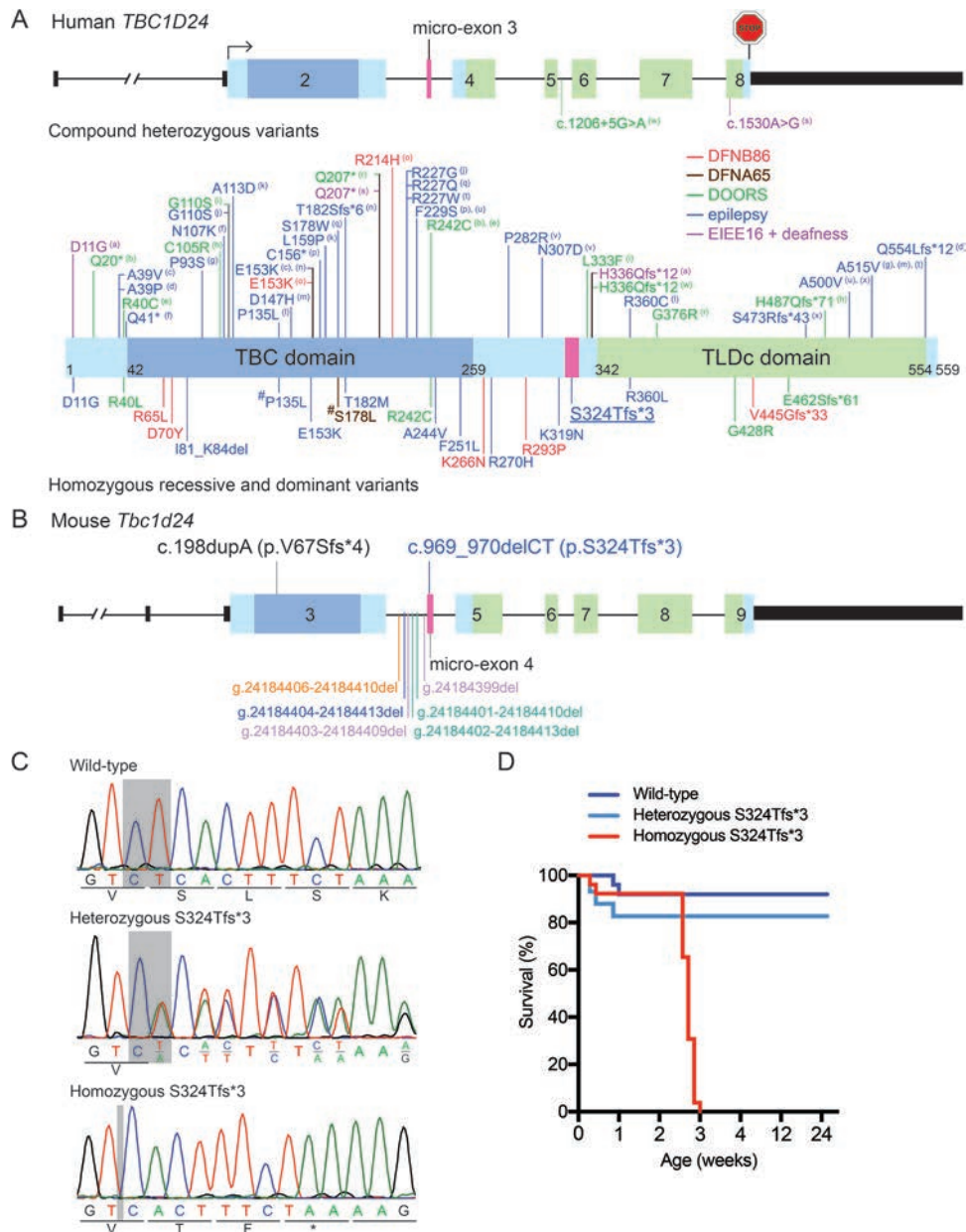


Figure 1. Human pathogenic variants of *TBC1D24* and CRISPR-Cas9 editing to engineer the S324Tfs*3 mutation of mouse *Tbc1d24*. (A) Structure of the human *TBC1D24* gene and the location of pathogenic variants in the encoded protein. The eight annotated exons of human *TBC1D24* are depicted with the seven protein-coding exons (colored rectangles). Exon 2 (blue) encodes the TBC domain (deep blue). Exons 4 to 8 encode the TLDC domain (light green). Alternatively spliced micro-exon 3 is shown in pink. The 5' untranslated sequence of exon 1 and part of exon 2 and 3' untranslated region of exon 8 are in black. A right-pointing arrow above exon 2 indicates the location of the translation start codon. A red stop sign marks the location of the translation start codon. Two reported pathogenic splice-site variants (mutations) of human *TBC1D24* are drawn below the gene structure. To date, an additional 55 variants that alter the *TBC1D24* protein are reported and have been depicted based upon the amino acid sequence of the longest isoform of *TBC1D24* (NM_001199107). Variants are grouped by color depending on the clinical phenotype. They have been associated with DFNB86 non-syndromic recessive deafness (red font), dominantly inherited non-syndromic deafness DFNA65 (brown), DOORS syndrome (green), epilepsy (blue) and EIEE16 epilepsy with deafness (purple). The same lowercase and superscripted letter written in parentheses identifies the two variants in compound heterozygosity. Homozygous recessive and dominant variants are drawn under the protein structure. The one-letter code for amino acids is used in this figure. For example, P135L indicates a leucine residue substituted for the wild-type proline. Two dominant variants are marked with a #. An asterisk indicates a stop codon, fs indicates a translation frameshift and the number after an asterisk indicates the number of mutant amino acids residues encoded in a different translation reading frame before the premature translation stop codon. The S324Tfs*3 mutation, the focus of this study, is underlined. References for all of these variants are provided in Table S1. (B) Structure of the mouse *Tbc1d24* gene. The longest reported isoform of mouse *Tbc1d24* (NM_001163847) is encoded by nine exons. In mouse, there are two 5' non-coding exons depicted as black rectangles prior to the first protein-coding exon 3. Coding regions are drawn as thick colored bars. The sequence encoding the TBC domain is deep blue, the sequence encoding the TLDC domain is green, the sequence of micro-exon 4 is red and the sequence encoding the remainder of the *TBC1D24* protein is light blue. Intronic regions are drawn as thin black lines. Two CRISPR-Cas9-generated *Tbc1d24* mutant alleles, V67Sfs*4 and S324Tfs*3 depicted above the drawing, were used in this study. The intended c.969_970delCT (p.S324Tfs*3) variant is located in alternatively spliced micro-exon 4 (g.24184399_24184395del; GRCh38/mm10). Six unintended variants located in the adjacent intron 3 sequence were also generated by the gRNA for S324Tfs*3. Blue, green and purple colors represent pairs of compound heterozygous alleles, while the variant of g.24184406-24184410del (orange) is found in homozygotes. (C) Representative DNA Sanger sequence traces are shown for the wild-type, heterozygous S324Tfs*3 and homozygous S324Tfs*3. (D) A Kaplan-Meier survival curve is shown from 1–24 weeks for wild-type (9 males and 16 females), heterozygous S324Tfs*3 (27 males and 31 females) and homozygous S324Tfs*3 (9 males and 17 females) mice.

Table 1. Human disorders associated with mutations of genes encoding of TBC domain-containing proteins

Gene	Name of disorders	Phenotype	OMIM
TBC1D1	obesity	Association of TBC1D1 polymorphism R125W with familial severe obesity	609850
TBC1D4	Type 2 diabetes susceptibility	Common Greenland variant of TBC1D4 confers muscle insulin resistance	612465
TBC1D20	WARBM	Bilateral congenital cataracts, microphthalmia, microcornea, optic atrophy, intellectual disability, axonal peripheral neuropathy and hypothalamic hypogonadism	611663
TBC1D23	PCH	Pontocerebellar hypoplasia, global hypotonia, gross and fine motor skill deficits and expressive and receptive language deficits	617687
TBC1D24	EIEE16, PME and FIME	EIEE16 with or without deafness, PME, FIME, respectively	615338, 310370 and 605021
	DOORS	Onychodystrophy, osteodystrophy, intellectual disability and seizures	220500
	DFNB86 and DFNA65	Non-syndromic deafness with recessive and dominant inheritance, respectively	614617 and 616044
TBC1D32/C6orf170	OFD (Orofaciodigital syndrome type IX)	Midline cleft, microcephaly, colobomatous microphthalmia/ anophthalmia, variable polydactyly, absent pituitary, congenital heart disease and abnormal inner ear	615867

Online Mendelian Inheritance in Man (OMIM; <https://www.omim.org>).

However, for lack of mutant vertebrate animal models of human TBC1D24 deficiency, the functions of this protein and the pathogenesis of TBC1D24 deficiency-related diseases are incompletely understood.

Our study of the *in vivo* functions of TBC1D24 was focused on engineering a mouse model of EIEE16. In humans, EIEE16 is characterized by early-onset epileptic encephalopathy refractory to therapy, seizures, ensuing neurological deterioration, and early death associated with homozygosity for a deletion of two nucleotides (c.969_970delGT) of TBC1D24. This mutation, designated S324Tfs*3, is predicted to cause a substitution of threonine (T) for the wild-type serine (S) at residue 324 followed by a translation frameshift (fs), resulting in a premature translation stop codon (*) three codons downstream. This rare recessive p.S324Tfs*3 allele is segregating in a large Turkish family (18,24,25) and is one of 55 reported pathogenic variants of human TBC1D24 (Fig. 1A, underlined variant). The S324Tfs*3 variant of TBC1D24 is located in alternatively spliced micro-exon 3 composed of 18 nucleotides, which encodes a peptide sequence perfectly conserved between human and mouse. To understand the function of TBC1D24, as well as the pathology associated with the c.969_970delGT (p.S324Tfs*3) variant, we used CRISPR-Cas9 (clustered regularly interspaced short palindromic repeats and CRISPR-associated protein) to edit the mouse genome and generate the same human recessive mutation associated with EIEE16. We observed that the phenotype of a homozygous S324Tfs*3 *Tbc1d24* mouse resembles human EIEE16. We also report a second CRISPR-Cas9-edited mouse with a recessive mutation (c.198dupA; p.V67Sfs*4) of *Tbc1d24* that causes a late embryonic lethality. *In situ* hybridization, using RNAscope probes, identified the regions of the brain expressing *Tbc1d24*. At the ultrastructural level, TBC1D24 protein is located in the trans-Golgi network (TGN) and at synapses, consistent with mammalian TBC1D24 having a function in vesicle trafficking important for signal transmission in neurons.

Results

Seizures of *Tbc1d24* mutant mouse resemble human TBC1D24-associated epileptic encephalopathy

The S324Tfs*3 variant of the mouse *Tbc1d24* gene generated in this study, using CRISPR-Cas9 editing (Fig. 1B and C), is identical to a mutation of human TBC1D24 associated with early-onset severe seizures. The S324Tfs*3 mutation is located in micro-exon 4 of mouse *Tbc1d24*, which is equivalent in sequence to human micro-exon 3. We engineered the S324Tfs*3 mutation using CRISPR-Cas9 editing. After obtaining germline inheritance of the S324Tfs*3 (Fig. 1B and C), we explored the phenotype of homozygous mutants. From birth, we monitored viability and seizures of S324Tfs*3 homozygotes ($n = 26$), heterozygotes ($n = 58$) and wild-type ($n = 25$) littermates.

Homozygous S324Tfs*3 mice exhibited spontaneous tonic-clonic seizures (Racine scale, stage 5) that were detected visually after 2 weeks of age (approximately P15). Abruptly by 3 weeks of age, all homozygous S324Tfs*3 mice died likely due to seizures or general prostration (Fig. 1D). Seizures in these homozygous S324Tfs*3 mice manifested as wild running (uncontrollable movement at high velocity), and then convulsions (muscle rigidity and jerking movements), followed by a postictal state (26–28). Heterozygous S324Tfs*3 mice did not have seizures indicating that S324Tfs*3 is a recessive allele in mice as it is in humans (24).

To quantitatively evaluate the seizure phenotype, continuous recordings of 27 mice were made for 30 min each day for 13 days. We observed homozygous S324Tfs*3 mice ($n = 9$), heterozygous S324Tfs*3 mice ($n = 10$) and their wild-type littermates ($n = 8$). The representative examples of 1 min tracking of a P17 wild-type mouse, a heterozygous S324Tfs*3 mouse and a homozygous S324Tfs*3 mouse are shown in Figure 2A. Each point indicates a position of an animal in a single recording frame, and the color reflects the animal's frame-by-frame

velocity (see also [Supplementary Material, Fig. S1 and Supplementary recording](#)). [Figure 2B](#) shows phases of seizure, and [Figure 2C](#) confirms that the homozygous S324Tfs*3 mouse (the same mouse as in [Fig. 2A](#)) had bouts of wild running during the 30 min recording. Some homozygous S324Tfs*3 mice exhibited obvious seizures at P15, and, by P17, nearly all homozygous S324Tfs*3 mice (7 of 9) experienced spontaneous seizures in the open-field environment during the 30 min recording sessions ([Fig. 2D](#)).

The mean velocities from the bin with the maximum velocity were plotted in [Figure 2E](#). To assess variables that influence these velocities in each genotype, a repeated measures ANOVA was performed with velocity as the dependent variable against three factors: age (P5, P7, P9, P11, P13, P15, P16 and P17), genotype (wild-type, heterozygous S324Tfs*3 and homozygous S324Tfs*3) and sex (male and female). Homozygous S324Tfs*3 mice showed high-velocity wild-running at P17 with no significant differences between male and female mice of each genotype ($P = 0.24$). Next, we compared movements during a normal state in homozygous S324Tfs*3 with wild-type and heterozygous S324Tfs*3. The mean distance traveled was similar for all three genotypes ([Fig. 2F](#)). We compared distance traveled in the homozygous S324Tfs*3 mice during the different phases of the seizure ([Fig. 2G](#)). In comparison to the pre-seizure state, the distance traveled during wild-running was considerably longer ($P < 0.0001$). Following wild-running, homozygous S324Tfs*3 mice displayed convulsions typified by immobility expressed as tonus, hindlimb extension and postictal state. The distance traveled during a convulsion and during the postictal state revealed a significantly shorter distance than that of wild running ($P < 0.0001$; [Fig. 2G](#)). Together, these results indicate that homozygous S324Tfs*3 mice have seizures and an early death, which resemble the phenotype of humans homozygous for the TBC1D24 S324Tfs*3 variant ([18,24,25](#)).

S324Tfs*3 mice have normal auditory and vestibular function

Deaf mutant mice may have a vestibular deficit that can manifest as running in circles and head-bobbing behavior ([29](#)). Some pathogenic variants of human TBC1D24 are associated with non-syndromic deafness, epilepsy with deafness and DOORS syndrome ([Fig. 1A](#)). However, there are no reports of a hearing deficit in human subjects homozygous for S324Tfs*3 ([24,25](#)). Nevertheless, we explored the possibility that the rapid movements of homozygous S324Tfs*3 mice could be due, entirely or in part, to a vestibular abnormality, perhaps coupled with a hearing deficit.

We quantitatively evaluated the hearing in mice using auditory brainstem responses (ABRs) and distortion product otoacoustic emissions (DPOAEs). ABRs for homozygous S324Tfs*3, heterozygous S324Tfs*3 and wild-type littermates at P17 were measured at 4 frequencies (8, 16, 32 and 40 kHz; [Fig. 3A](#)). ABR responses were detected within normal range for each of the three genotypes. Homozygous S324Tfs*3 mice and their littermate controls also showed normal DPOAEs indicating normal outer hair cell function ([Fig. 3B](#)). Next, we evaluated vestibular function of P16 homozygous S324Tfs*3 mice and controls (heterozygotes and wild-type littermates) using vestibular sensory-evoked potentials (VsEPs). Homozygous S324Tfs*3 mice had VsEP thresholds indistinguishable from the VsEPs of wild-type and heterozygous littermate controls ([Fig. 3C](#)). Taken together, these data indicate that the wild-running of homozygous S324Tfs*3 mice is not due

to a vestibulopathy but is associated with seizures. We also performed morphological evaluations of inner ear sensory epithelia of wild-type and homozygous S324Tfs*3 mice. Representative images of the middle turn of the cochlea are shown in [Figure 3D](#). As expected from ABR, DPOAE and VsEP analyses, wild-type and homozygous S324Tfs*3 sensory epithelia were structurally indistinguishable along the entire cochlear length.

Tbc1d24 mRNA expression in brain and specificity of TBC1D24 antibody

An RNAscope probe (Probe-Mm-Tbc1d24) was used for in situ hybridization to identify cell types that express *Tbc1d24* mRNA in the wild-type mouse brain. *Tbc1d24* mRNA was readily detected in P17 and P30 wild-type mice, in the CA1-CA3 region of the hippocampus, dentate gyrus (DG), cerebral cortex (CC) and olfactory bulb (OB) ([Fig. 4A](#)), corroborating published data ([10](#)). *Tbc1d24* mRNA expressed by homozygous S324Tfs*3 mice at P17 was localized in the same regions but at a lower expression level compared with the wild-type littermate control ([Fig. 4A](#); [Supplementary Material, Fig. S2A](#)). Transcripts that include or exclude micro-exon 4 of *Tbc1d24* would both be detected by in situ hybridization with our RNAscope probe. The reduced RNAscope signal for *Tbc1d24* transcripts of S324Tfs*3 homozygous mice compared to the wild-type (processed simultaneously and identically) may be explained by a transcriptional reduction of *Tbc1d24* mRNA that does not include exon 4 ([Fig. 4A](#); [Supplementary Material, Fig. S2A](#)), by the predicted nonsense-mediated decay (NMD) ([30](#)) of *Tbc1d24* transcripts that include micro-exon 4 harboring the S324Tfs*3 mutations or both events.

Blind to genotype, we next evaluated histopathology in brains of homozygous S324Tfs*3 mice and wild-type control littermates at P14 and P17. The gross anatomy of brains from homozygous S324Tfs*3 mice appeared to be normal ([Supplementary Material, Fig. S2B](#)). As seizures in homozygous S324Tfs*3 mice were only observed after P15, cross sections of the OBs, CC, hippocampus, DG, thalamus, brainstem and cerebellum were also evaluated after hematoxylin and eosin staining at P17. These regions of the brain at P17 from homozygous S324Tfs*3 mice had a normal gross morphology indistinguishable from the wild-type ([Supplementary Material, Fig. S2B](#)). Magnetic resonance imaging (MRI) *ex vivo* revealed no difference in the gross morphological features between homozygous S324Tfs*3 mice and wild-type littermates ([Supplementary Material, Fig. S2C](#)).

The intracellular localization of TBC1D24 protein was determined using a commercial antiserum (Novus NBP1-82925). The epitope used to raise this antiserum was 77 residues (51–127, NP_001186036) of human TBC1D24. The amino acid sequence of this epitope is 94.8% identical to the same region of mouse TBC1D24 ([Fig. 4B](#)). To evaluate the specificity of this human antibody against mouse TBC1D24, we performed immunohistochemistry and immunoblotting using brain from a CRISPR-Cas9-edited homozygous *Tbc1d24* of V67Sfs*4 mouse ([Supplementary Material, Fig. S3A](#)) and wild-type littermate controls. In mouse *Tbc1d24*, the epitope of this antibody includes residues 51–127 encoded by exon 3 (NP_001157319). The CRISPR-Cas9-edited V67Sfs*4 (c.198dupA) allele changes the translation reading frame at residue 67 ([Fig. 4B](#)). Thus, only 17 residues could remain at the N-terminus of this epitope in a mouse homozygous for the V67Sfs*4 allele. If a truncated TBC1D24 protein is made, these 17 residues might be recognized by the antiserum against TBC1D24. However, such a truncated

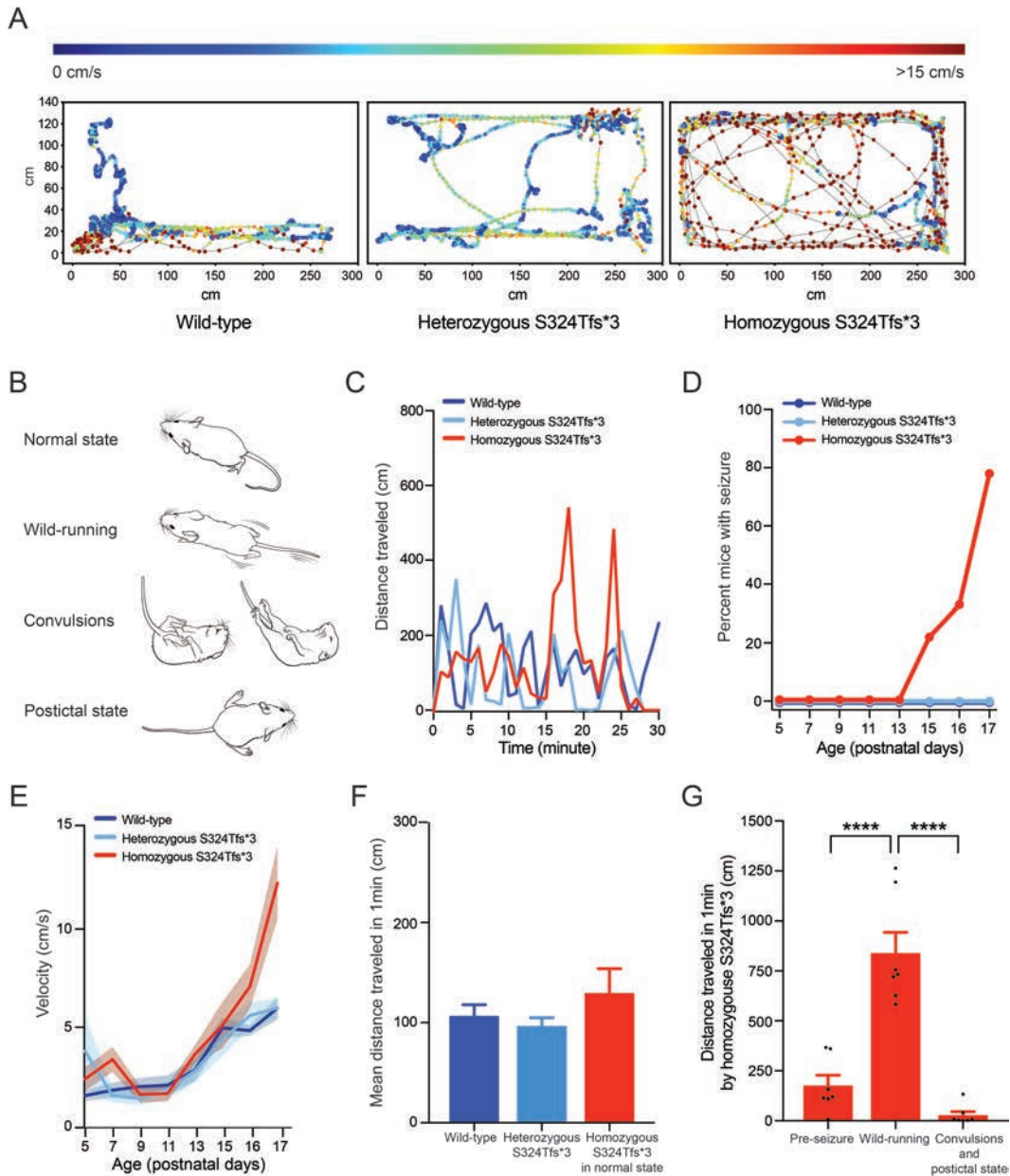


Figure 2. Homozygous *Tbc1d24* S324Tfs*3 mice in an open-field environment exhibit spontaneous tonic-clonic seizures. (A) An example of 1 min positions of P17 wild-type (left), heterozygous S324Tfs*3 (middle) and homozygous S324Tfs*3 (right) mice. Each point represents the position of a mouse in the cage in a single video frame (30 frames per s). The color of the dot indicates the relevant frame-by-frame velocity with hotter colors indicating higher velocities. These 1 min time intervals are numerically flagged for each session as containing the highest velocity in the test session (see [Materials and Methods](#) for details). (B) Representative mouse images during seizure. Seizure of homozygous S324Tfs*3 mice begins with wild-running (uncontrollable movement at high velocity), and then convulsions (hindlimb flexion, hindlimb extension and jerking movements), followed by a postictal state. (C) Examples of distance traveled per 1 min for a wild-type, heterozygous S324Tfs*3 and homozygous S324Tfs*3 mouse at P17. The homozygous S324Tfs*3 mouse shows two peaks of high velocity (long distance traveled) typical of wild-running followed by convulsion and postictal state. (D) Homozygous S324Tfs*3 mice begin having obvious spontaneous seizures at approximately P15. The majority of homozygous S324Tfs*3 mice (7 out of 9) are observed having seizures at P17 during the 30 min long recording. (E) The average velocity (\pm SEM) within the 1 min bin with the maximum within session velocity as a function of postnatal age. (F) Movements of normal state (no obvious seizures) of homozygous S324Tfs*3 mice at P17 were compared with wild-type and heterozygous S324Tfs*3 mice using the mean distance traveled in 1 min. Distance traveled is similar in all three groups. (G) In homozygous S324Tfs*3 mice with seizures at P17 ($n = 7$), velocity during pre-seizure, wild-running and convulsions and the postictal state were compared using the total distance traveled in 1 min. Statistical analyses were performed using a one-way ANOVA with repeated measures followed by a *post hoc* test. The distance traveled during wild-running is significantly longer than during the pre-seizure phase. The distance traveled during convulsions and the postictal state shows significantly lower velocities compared to the wild-running state. Error bars are means \pm SEM; **** $P < 0.0001$.

protein would be an exception as the mRNA with the V67Sfs*4 premature translation stop codon in exon 3 would likely be subjected to NMD (30).

Since homozygosity for the V67Sfs*4 allele results in perinatal lethality, brains were dissected from E18.5 embryos obtained from matings between heterozygous mice. Protein was

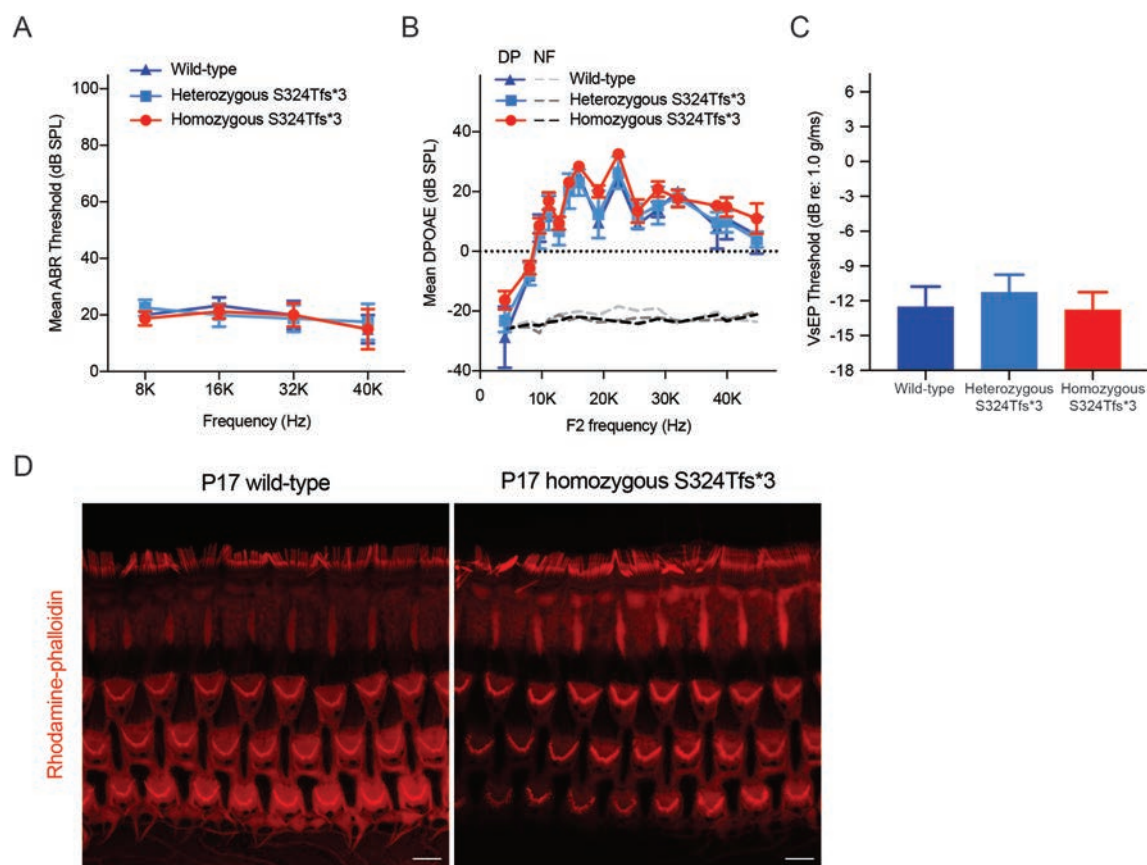


Figure 3. Auditory and vestibular functions of homozygous *Tbc1d24* S324Tfs*3 mice at P16–P17. (A) Mean ABR thresholds of wild-type ($n = 3$), heterozygous S324Tfs*3 ($n = 4$) and homozygous S324Tfs*3 ($n = 4$) littermate mice at P17. Homozygous S324Tfs*3 mice have normal hearing at P17. (B) Mean DPOAE levels for the same mice tested with ABRs are indistinguishable from the wild-type. Black and gray dash lines indicate noise floors. (C) Mean VsEP thresholds of wild-type ($n = 3$), heterozygous S324Tfs*3 ($n = 4$) and homozygous S324Tfs*3 mutant mice ($n = 4$) at P16. Homozygous S324Tfs*3 mutant mice have normal functioning vestibular and auditory systems at P16–P17. All data represent mean \pm SD. (D) Rhodamine-phalloidin (red) staining of filamentous actin structures of P17 wild-type and homozygous S324Tfs*3 mouse auditory sensory epithelium of the cochlear middle turn showing normal morphology of three rows of outer hair cell and one row of inner hair cell stereocilia. Scale bars are 5 μ m.

isolated from the dissected brains, and DNA was extracted from each embryo for genotyping. Immunoblotting analysis using the TBC1D24 antibody revealed a band at the predicted size (63 kDa) in the wild-type brain sample (Supplementary Material, Fig. S3B). However, in a protein sample from the brain of a homozygous V67Sfs*4 mouse, the 63 kDa band was absent (Supplementary Material, Fig. S3B). A band corresponding to α -tubulin, used as a loading control, was present in all lanes. Thus, the antiserum against human TBC1D24 is specific for the 63 kDa protein and shows little or no cross-reactivity with other proteins in the mouse brain. The specificity of this antibody was also confirmed using cryosections of E18.5 wild-type brain in which TBC1D24 immunoreactivity was localized to the hippocampus and DG, whereas a TBC1D24 signal was absent in these parts of brain from a homozygous V67Sfs*4 mouse (Supplementary Material, Fig. S3C).

Immuno-transmission electron microscopy reveals TBC1D24 localization in TGN and at synapses in the hippocampus

At the ultrastructural level, the intracellular localization of TBC1D24 was determined by immuno-transmission electron microscopy (TEM) using the primary TBC1D24-specific antibody

and a gold-conjugated secondary antibody (Fig. 4C–H) and focusing on neurons of the hippocampus, since this region expressed *Tbc1d24* mRNA as revealed using an RNAscope probe. TBC1D24 was detected in the TGN, enriched at clathrin-coated vesicles, identified by their characteristic ultrastructure (Fig. 4C and D). The lattice of clathrin triskelia is readily evident in electron microscopy of the TGN. Gold particles appear as black dots (Fig. 4C–H). Labeling was also evident at synapses, both presynaptic (Fig. 4E–I) and postsynaptic (not shown). In most cases, gold particles at synapses appeared to be concentrated in vesiculate structures and at possible sites of endocytosis. These latter sites include the ends of invaginating spinules, which are structures involved in endocytosis (Fig. 4E and I) (31), and sites associated more directly with the presynaptic membrane active zone (Fig. 4F and I) or adjacent to it. This region of the presynaptic terminal is involved in synaptic vesicle recycling (32). These data suggest an association of TBC1D24 with vesicle trafficking in the neuron.

Seizure onset correlates temporally with SRRM3-dependent inclusion of the *Tbc1d24* micro-exon

Human TBC1D24 alternatively spliced micro-exon 3 is equivalent in sequence to all but 1 of the 18 nucleotides of mouse

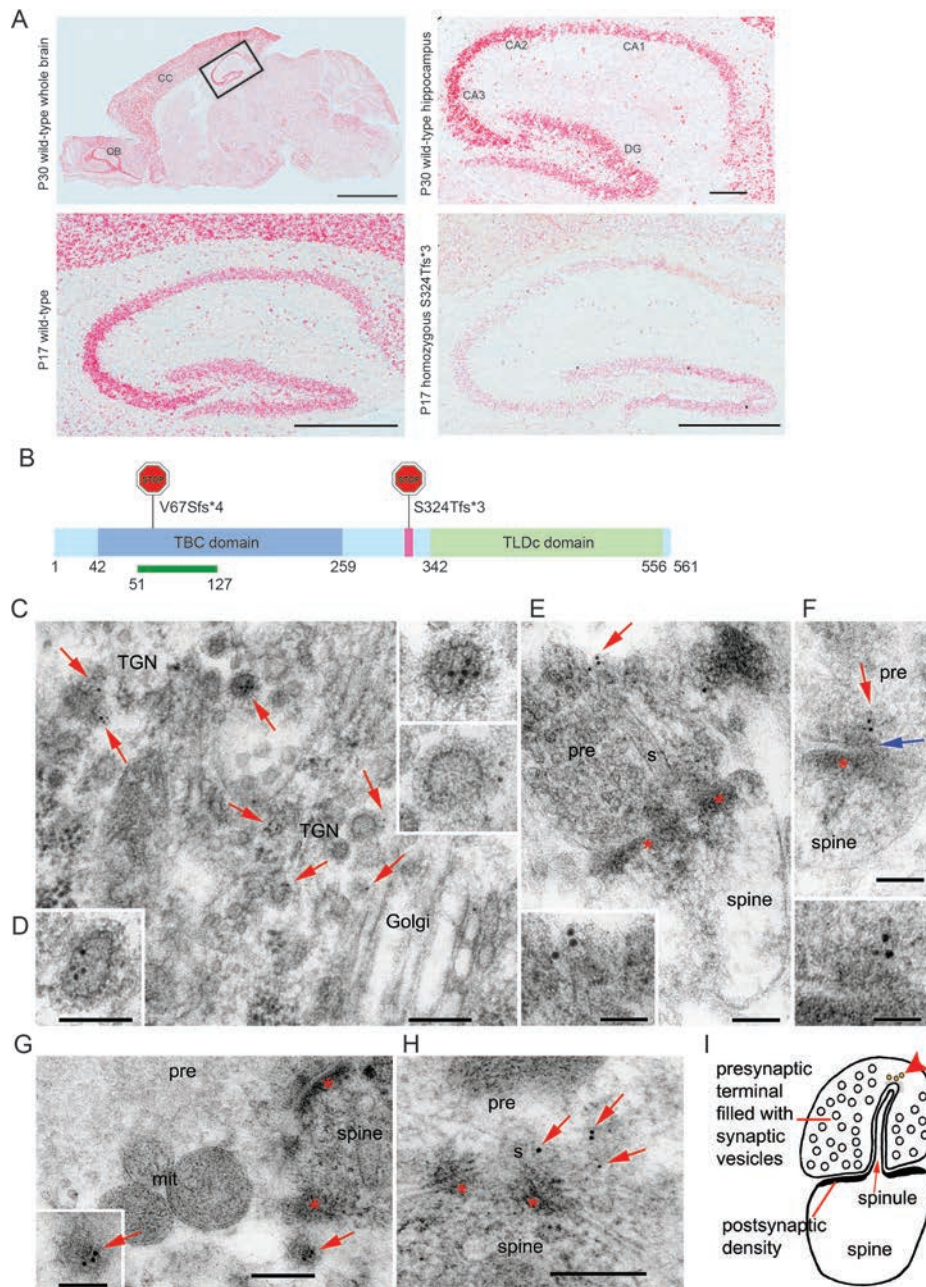


Figure 4. Expression of *Tbc1d24* mRNA and TBC1D24 protein in the hippocampus and DG. (A) *In situ* hybridization using RNAscope Probe-Mm-Tbc1d24 in a wild-type mouse at P30. *Tbc1d24* mRNA is abundant in the hippocampus, DG, CC and OB (upper left panel). Upper right panel is an enlarged image of the hippocampal area indicated by the black rectangle. *Tbc1d24* mRNA is highest in the CA3. *Tbc1d24* mRNA expression of homozygous S324Tfs*3 mice at P17 is detected in the same regions (lower right panel) but with lower expression level compared with wild-type littermate control (lower left panel). Scale bars are 2000 μ m (upper left panel), 200 μ m (upper right panel) and 500 μ m (lower panels). (B) Mouse TBC1D24 protein structure (NP_001157319) showing the locations of the premature translation stop codons resulting from the V67Sfs*4 and S324Tfs*3 variants. A green bar corresponds to the location of the epitope used to raise the TBC1D24 antibody. The epitope of the antibody (Novus NBP1-82925) is 77 residues of human TBC1D24 (amino acids 51–127; NP_001186036) of which 73 residues are identical to mouse TBC1D24. (C–F) Immunogold electron microscopy of thin sections of the hippocampus labeled with antibody to TBC1D24 and 10 nm immunogold (CA1 stratum radiatum–pyramidale). In neuron somas, labeling (red arrows) is concentrated in the TGN (C and D), especially at clathrin-coated vesicles. In the magnified insets, two clathrin-coated vesicles have five and two gold particles. Labeling also is prevalent at synapses (E and F), which have three gold particles labeling vesiculate structures near the distal end of an invaginating spinule (s in E) and a small invagination of the presynaptic membrane (blue arrow in F). See also the magnified image of three gold particles in the insets to (E) and (F). TGN, *trans*-Golgi network; pre, presynaptic terminal; spine, postsynaptic spine; s, invaginating spinule; asterisk, postsynaptic density. Scale bars are 200 nm in (C), 100 nm in (D) (and for insets in (C), (E) and (F)) and 50 nm in insets in (E) and (F). (G and H) Immunogold labeling in the CA3 stratum lucidum mossy terminal synapses. The mossy terminals (pre) are filled almost completely with synaptic vesicles (evident in G), as well as mitochondria (mit). The postsynaptic structures are thorny excrescences, which are modified spines (spine). In (G), the lower edge of the spine and postsynaptic density (asterisk) is very oblique, and a rounded structure in the adjacent presynaptic cytoplasm is labeled with three gold particles (see inset; its size and shape suggest that it is the surface of a clathrin-coated vesicle). In (H), gold-labeling in the mossy terminal is associated with a spinule (s). Scale bars are 200 nm in (G) and (H) and 100 nm in the inset. (I) The diagram illustrates a typical postsynaptic spine with a spinule invaginating into a presynaptic terminal, as shown in (E); often, a clathrin-coated vesicle forms on the distal end of the spinule invagination (31), but this distal area is not distinct in (E). Three gold dots represent the interpreted position of the three gold particles near the distal end of the spinule evident in the synapse in (E).

Tbc1d24 micro-exon 4, and both encode identical amino acid residues (Fig. 1A and B; Supplementary Material, Fig. S4C). Since the S324Tfs*3 mutation is present in micro-exon 4 of mouse *Tbc1d24*, only transcripts of *Tbc1d24* that include this micro-exon carry the S324Tfs*3 mutant allele. For both human and mouse, exclusion of the micro-exon sequence in transcripts from S324Tfs*3 homozygotes will result in wild-type mRNA and will produce a wild-type, slightly smaller TBC1D24 protein isoform.

To evaluate the extent and developmental timing of alternative splicing of the mouse micro-exon 4, the ratio of micro-exon 4-containing and -omitting splice forms of *Tbc1d24* were analyzed in the mouse brain at E14.5, P1, P7, P16 and P30 using RT-PCR (Fig. 5A–C). This analysis revealed a postnatal switch in the expression of the two splice forms of *Tbc1d24*. At E14.5 and P1, the micro-exon 4-omitting transcript was the predominant splice form of *Tbc1d24* (Fig. 5B). In contrast, at P7 and later times, the predominant splice form of *Tbc1d24* mRNA contained micro-exon 4. Next, we used qRT-PCR to quantify the incorporation of micro-exon 4 into the *Tbc1d24* mRNA in the brain cortex of wild-type mice at E14.5, E18.5 and P16 (Fig. 5D). The expression of the micro-exon 4-containing splice form was normalized to the total transcript level of *Tbc1d24*. The qRT-PCR analysis demonstrated that the incorporation of micro-exon 4 into *Tbc1d24* increased approximately 23-fold in the brain cortex between E18.5 and P16. At E14.5 and E18.5, the expression levels of the micro-exon 4-containing splice form were similar (Fig. 5D). Together, these data indicate that the expression of the isoform of *Tbc1d24* containing micro-exon 4 increases dramatically in brain during early postnatal development and precedes by a few days the abrupt onset of seizures.

A search of GenBank entries for mouse *Tbc1d24* mRNA revealed that the micro-exon 4 of *Tbc1d24* was spliced into the mRNA selectively in neural tissues. Therefore, we chose to test neuron-specific regulators of alternative splicing from three families of splicing factors for their abilities to affect the incorporation of micro-exon 4 into the mature mRNA in minigene-based splicing assays. Specifically, a *Tbc1d24* minigene was generated by subcloning micro-exon 4 and its flanking introns between two constitutively spliced exons of an exon-trap vector, and the non-neuronal cell line HEK293 was co-transfected with the minigene and a plasmid encoding the neuronal splicing factor NOVA1, RBFOX1, SRRM3 or SRRM4 (Fig. 5E). Negative control HEK293 cells were co-transfected with the minigene and the empty vector. Splicing of the minigene-encoded transcript was analyzed by RT-PCR using primers that annealed to the constitutive exons of the minigene. This analysis revealed that the transfection of HEK293 cells with either SRRM3 or SRRM4 increased the inclusion of micro-exon 4 into the minigene-encoded transcript. In contrast, transfection of HEK293 cells with either NOVA1 or RBFOX1 did not affect the splicing of micro-exon 4. Thus, SRRM3 and SRRM4 regulate the alternative splicing of micro-exon 4 in transfected cells.

Next, we tested *in vivo* whether SRRM4 or the closely related splicing factor SRRM3 regulated the alternative splicing of *Tbc1d24*. RNA was isolated from the brain cortex of *Srrm4*-deficient mutant mice (*Srrm4*^{bu/bu}) (33), wild-type mice and *Srrm3* gene-trapped, SRRM3-deficient mice (*Srrm3*^{gt/gt}; Y. Nakano and B. Banfi, manuscript in preparation) at P16. RT-PCR analysis of the isolated RNA demonstrated that the ratio of the micro-exon 4-containing versus micro-exon 4-omitting splice forms of *Tbc1d24* was abnormally low in the brain cortex of *Srrm3*^{gt/gt} mice but not in that of *Srrm4*^{bu/bu} mice (Fig. 5F). Thus, although the

inclusion of micro-exon 4 of *Tbc1d24* into the mature transcript is supported by both SRRM3 and SRRM4 *in vitro* (Fig. 5G), *in vivo* SRRM4 cannot maintain the alternative splicing regulation of *Tbc1d24* micro-exon 4 in the absence of SRRM3 (Fig. 5H). These data indicate that SRRM3 is at least one of the splicing factors required for the wild-type regulation of the alternative splicing of micro-exon 4 of *Tbc1d24* in the brain cortex.

Although *Tbc1d24* mRNA (Supplementary Material, Fig. S4A) and protein (5) are expressed in spiral ganglion neurons of the inner ear, the S324Tfs*3 mutations of human TBC1D24 and mouse *Tbc1d24* are not associated with hearing loss (24,25) (Fig. 3A and B). Based on these data, we hypothesized that micro-exon 4 was not spliced into the majority of *Tbc1d24* transcripts in the inner ear. To test this hypothesis, we performed RNA-seq analyses of wild-type mouse cochleae, which revealed that some transcripts of *Tbc1d24* include and other transcripts exclude micro-exon 4 at E16.5, P0 and P49 (Supplementary Material, Fig. S4B). Perhaps, in the auditory system of S324Tfs*3 homozygotes there is a sufficient amount of wild-type TBC1D24 protein translated from transcripts lacking the micro-exon-encoded six residues that allows for normal hearing. The question still remains as to whether or not the splice isoform of TBC1D24 that includes the additional six residues encoded by the micro-exon (Supplementary Material, Fig. S4C) is necessary for normal brain function in mouse and human.

Discussion

Epilepsy, defined as recurrent, unprovoked seizures, occurs in ~50 million people worldwide and may be co-morbid with autism, schizophrenia and intellectual impairment. A genetic etiology is posited for a majority of individuals with epilepsy, and rare pathogenic mutations in approximately 40 different genes are associated with inherited forms of epilepsy. One such gene is TBC1D24. Mutations of human TBC1D24 are associated with a spectrum of neurological and skeletal disorders including intellectual disability, deafness, seizures, onychodystrophy and osteodystrophy (Fig. 1A). The *in vivo* pathogenic mechanisms that give rise to these disorders and the wild-type functions of TBC1D24 are not well understood, in part, for lack of mammalian animal models that recapitulate each of these distinct clinical phenotypes. In rat, Falace *et al.* electroporated shRNA targeting *Tbc1d24* mRNA in E15 embryos in the uterine horn to knockdown TBC1D24 protein and observed a delay in radial migration and defective terminal branching of pyramidal neurons (22). Using CRISPR-Cas9 editing of mouse *Tbc1d24*, we have begun to address this deficit and describe the first viable mouse that has the identical pathogenic variant and the same recurring, spontaneous seizure phenotype to that described in human subjects with EIEE16. Similar to the human family with early-onset epileptic encephalopathy (24,25), the homozygous S324Tfs*3 mouse model has normal hearing and vestibular function and tonic-clonic seizures along with an early death by P20. Heterozygous S324Tfs*3 mice have a normal lifespan, do not have seizures and otherwise appear to be wild-type. Thus, S324Tfs*3 is a recessive allele.

There were four reasons we chose to engineer the S324Tfs*3 variant of the *Tbc1d24* gene in the mouse genome, so that it was the precise equivalent to a compelling pathogenic mutation of human TBC1D24 associated with early-onset severe seizures. First, in a large family segregating early-onset epileptic encephalopathy, there was statistically significant evidence of linkage of this neurological disorder to human chromosome 16pter-p13.3 (25), the location of the TBC1D24 gene. Second,

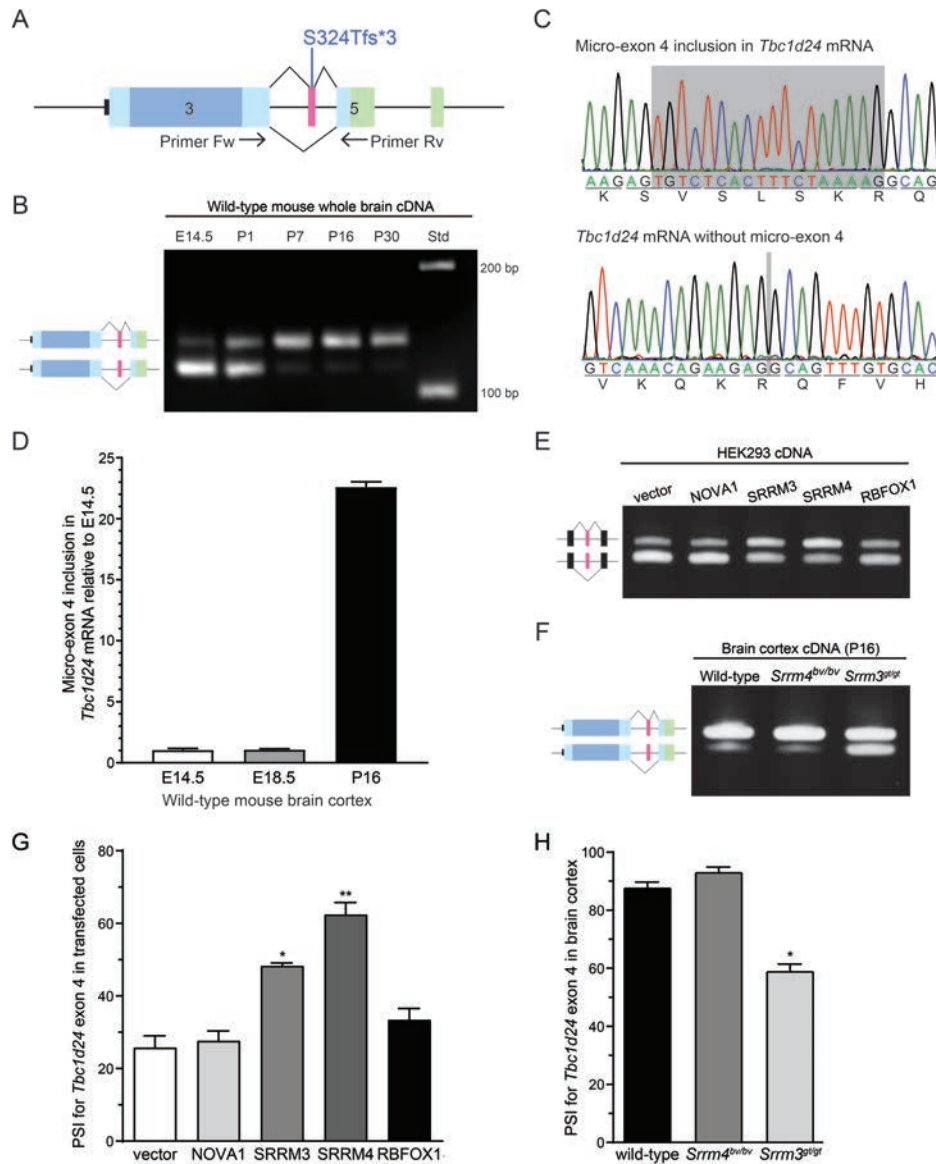


Figure 5. Alternatively spliced micro-exon 4 of mouse *Tbc1d24* is regulated by SRRM3. (A) Schematic of the alternative splicing of micro-exon 4 of mouse *Tbc1d24* pre-mRNA. A red vertical line indicates the location of the S324Tfs*3 variant. Arrows show the positions of PCR primers used in (B), (E) and (F). In homozygous S324Tfs*3 mice, *Tbc1d24* transcripts that exclude micro-exon 4 have a wild-type sequence. (B) Amplimers at E14.5, P1, P7, P16 and P30 of 135 bp include micro-exon 4, while 117 bp amplimers do not include the micro-exon 4 sequence. Qualitatively, inclusion of micro-exon 4 in the *Tbc1d24* mRNA increases with age in the brain of wild-type mice, and the long splice form becomes the predominant *Tbc1d24* transcript after P7. (C) Representative DNA Sanger sequence traces are shown for the two splice forms of *Tbc1d24*. (D) qRT-PCR analysis of the alternative splicing of micro-exon 4 of *Tbc1d24* in the brain cortex of wild-type mice at the indicated times. Expression of the micro-exon 4-containing splice form was normalized to the total transcript level of *Tbc1d24* at each time point. Error bars are mean \pm SEM. (E) RT-PCR testing of the splicing of micro-exon 4 in HEK293 cells co-transfected with a *Tbc1d24* minigene and an empty expression vector (vector) or the indicated neuronal splicing factor. (F) RT-PCR analysis of the alternative splicing of micro-exon 4 of *Tbc1d24* in the brain cortex of wild-type, *Srrm4^{bu/bv}* (Bronx waltzer) and *Srrm3^{gt/gt}* mice at P16. Inclusion of micro-exon 4 in *Tbc1d24* was reduced in the *Srrm3^{gt/gt}* samples but not in the *Srrm4^{bu/bv}* sample. (G) Quantification of the alternative splicing of micro-exon 4 of *Tbc1d24* in HEK293 cells co-transfected with the indicated splicing factors and a *Tbc1d24* minigene. The expression of minigene-encoded transcripts was analyzed by RT-PCR (E), and alternative splicing was quantified based on the band intensity of the longer (micro-exon 4-containing) RT-PCR product relative to the summed band intensities of the longer and shorter RT-PCR products (PSI). Values are mean \pm SEM ($n = 3$; one-way ANOVA, $P < 0.0001$; Dunnett's post hoc test, * $P = 0.0008$, ** $P < 0.0001$; control group, vector). (H) Quantification of *Tbc1d24* micro-exon 4 splicing in the brain cortex of mice of the indicated genotypes at P16. The expression of *Tbc1d24* splice forms was analyzed by RT-PCR (F), and alternative splicing was quantified based on the band intensity of the longer (micro-exon 4-containing) RT-PCR product relative to the summed band intensities of the longer and shorter RT-PCR products (PSI). Values are mean \pm SEM ($n = 3$; one-way ANOVA, $P < 0.0001$; Dunnett's post hoc test, * $P = 0.0002$; control group, wild-type).

affected individuals in this family were homozygous for the S324Tfs*3 variant and heterozygous carriers did not have seizures indicating that this mutant allele is recessive (25). Third, the S324Tfs*3 variant is located in an evolutionarily conserved, alternatively spliced micro-exon. *TBC1D24* transcripts that do not include the micro-exon will produce a wild-type shorter

protein isoform both in humans and mice homozygous for S324Tfs*3. We hypothesized that a mix of wild-type and mutant *Tbc1d24* transcripts would increase the likelihood that a mouse homozygous for S324Tfs*3 would be viable, having already observed that two other homozygous mutant alleles of mouse *Tbc1d24* that we obtained [*Tbc1d24^{tm1a}(EUCOMM)*Hmgu

and *Tbc1d24^{tm1b(EUCOMM)Hmgu}* or engineered with CRISPR-Cas9 (V67Sfs*4) were lethal embryonically. Finally, reducing or blocking the inclusion of the micro-exon harboring the S324Tfs*3 in *TBC1D24* transcripts using, for example, allele-specific oligos, might eventually be a therapeutic option in patients and could be explored in our mouse model of this specific mutant allele.

In making mutant animal models by editing the genome with the CRISPR-Cas9 system, there is ongoing debate about the extent of unintended off-target and on-target mutagenesis (34). The guide RNAs we used generated a single copy of the expected on-target S324Tfs*3 (c.969_970delCT) allele in compound heterozygosity with a 10-nucleotide deletion. There were also five additional on-target but unintended lesions in trans configuration that arose in three littermates of the S324Tfs*3 founder mouse and were subsequently eliminated by outcrossing the S324Tfs*3 (Fig. 1B). The unintended on-target lesions were located 4–18 bp upstream of the intended *Tbc1d24* target, an observation similar to genome editing reported for the mouse *Piga* gene (35). Refinement of the CRISPR-Cas9 system is needed to avoid similar unintended lesions for therapeutic editing of human inherited disorders.

The S324Tfs*3 variant of human *TBC1D24* is located in the 18 nucleotides of micro-exon 3 that is alternatively spliced and encodes an identical peptide sequence to that of mouse micro-exon 4. Analyses of cDNA made from mRNA extracted from wild-type mouse brain revealed that expression of the *Tbc1d24* isoform containing micro-exon 4 increases during postnatal development. The majority of the fetal transcripts from *Tbc1d24* do not include micro-exon 4. Fetal transcripts of mutant mice homozygous for the S324Tfs*3 of *Tbc1d24* that do not include micro-exon 4 have a wild-type sequence. However, the *Tbc1d24* transcripts that include the micro-exon are the predominant isoform in the adult brain. Homozygous S324Tfs*3 mutant mice were born and developed normally during the perinatal stage, but then abruptly began to exhibit tonic-clonic seizures, and all of them died by P20. The time of appearance of micro-exon 4 carrying the S324Tfs*3 in *Tbc1d24* transcripts correlates with the timeline of seizure onset. We hypothesize that timing of inclusion of this micro-exon into the mature *Tbc1d24* mRNA explains the abrupt onset of seizures after P15 and may also explain the onset of seizures in humans homozygous for this mutation. Reducing the inclusion of the micro-exon in *TBC1D24* may delay the onset and reduce the severity of seizures.

Seizures in humans and mice due to homozygosity for S324Tfs*3 do not address the question of whether or not the inclusion of the wild-type micro-exon-encoded peptide is necessary to achieve a normal phenotype. This could be tested in future studies by engineering a conditional allele that allows for selective deletion of micro-exon 4. In addition, a conditional tissue-specific knockout allele of the entire *Tbc1d24* gene could be used to determine if seizures are due to loss of *Tbc1d24* function in the hippocampus, arise from other regions of the brain or both.

Four families of alternative splicing factors are known to be critical for strictly neuron-specific regulation of alternative splicing: the NOVA, the RBFOX, the SRRM3/SRRM4 and the PTBP families (36) (Y. Nakano and B. Banfi, manuscript in preparation). Of the four families, PTBP is unique in that there is a switch from the expression of a non-neuronal paralog (PTBP1) to the expression of a neuronal one (PTBP2) during CNS development. In contrast, members of the other three families are upregulated during neuronal differentiation. From these three families, we selected only four proteins to test their effect on the alternative splicing of *Tbc1d24* micro-exon 4 in HEK293 cells

because paralogs within the three protein families have nearly indistinguishable molecular activities *in vitro*. However, in all three families, the redundancy *in vivo* is incomplete. This could potentially be due to the amounts of individual paralogs being insufficient *in vivo* to support alternative splicing of targets that bind to the splicing factors with low affinity. Alternatively, neuronal expression of paralog-specific interacting proteins may alter the exon 'preference' of the splicing factors in ways that are not apparent in heterologous expression systems. The effects of SRRM3 and SRRM4 on the alternative splicing of micro-exon 4 of *Tbc1d24* are also not identical in transfected cells versus the CNS. In transfected HEK293 cells, both SRRM3 and SRRM4 support the splicing of *Tbc1d24* micro-exon 4 into the mature transcript, whereas in the CNS SRRM4 cannot maintain the alternative splicing regulation of *Tbc1d24* micro-exon 4 in the absence of SRRM3.

The peptide sequence encoded by the micro-exon of *TBC1D24* is perfectly conserved between human and mouse (Supplementary Material, Fig. S4C) and contains three serine residues that are predicted to be phosphorylated. Ser322 is a canonical phosphorylation motif for GSK3 (37). Ser326 is part of a canonical CK1 phosphorylation motif (38) (Supplementary Material, Fig. S4C) suggesting that these residues provide predicted phosphorylation sites that could be functionally important and experimentally tested with point mutations of these serine residues.

Our study showed that *Tbc1d24* mRNA is widespread in the brain, with high levels in the hippocampus, DG, CC and OB. Immuno-TEM analysis in hippocampal neurons revealed *TBC1D24* localization in the TGN and synapses. Thus, there is a correlation between mRNA distribution and EM immunogold localization of *TBC1D24* throughout neurons, including in synapses. Seizures are linked to synaptic activity (39,40), and the hippocampus has been implicated in temporal lobe epilepsy (41,42), although we did not examine these latter correlations directly in this study. Hippocampal sclerosis characterized by atrophy, induration, neuronal loss and astroglial proliferation has also been reported in 65–70% of patients with temporal lobe epilepsy (43,44). Human variants of *TBC1D24* have been associated with various types of epilepsy including myoclonic epilepsy, epileptic encephalopathy, multifocal epilepsy and temporal lobe epilepsy (4,18,45,46). An MRI of 1 affected human subject homozygous for the S324Tfs*3 variant revealed diffuse brain atrophy at 31 months of age. The atrophy was especially severe in the right hippocampus (18,24). Our results suggest that some types of epilepsy due to mutations of *TBC1D24* might be caused by dysfunction of hippocampal neurons, where *TBC1D24* appears to have a role in vesicle protein trafficking and synaptic transmission. In mouse neuroblastoma cell line N2A, the *Tbc1d24* gene was knocked out with CRISPR-Cas9, and these cells were found to be more sensitive to oxidative stress and have reduced neurite outgrowth (47). Additionally, for a heterozygous *Tbc1d24^{tm1b}* mouse from EUCOMM (European Conditional Mouse Mutagenesis Program) haploinsufficient for *TBC1D24* *in vivo*, hearing was normal but there was an increase in volume of presynaptic endosome-like structures in cortical neuron cultures, indicating that *TBC1D24* modulates endosomal dynamics at the synapse (47), consistent with our observation on the immuno-TEM localization of *TBC1D24* associated with clathrin-coated vesicles and presynaptic vesiculate structures at possible sites of endocytosis.

Mutant alleles associated with each of the distinct *TBC1D24* disorders (deafness, epilepsy and DOORS) are located in sequences encoding the TBC domain, in the TLDC domain and

even in the spacer sequence that links these two domains (Fig. 1A). Although the more severe *TBC1D24* phenotypes are associated with nonsense, frameshift and splice-site mutations (18), some missense mutations are associated with a severe phenotype. For example, the amino acid substitution S178L was a dominant allele associated with non-syndromic deafness (DFNA65) (8,9), while P135L (48) (Fig. 1A) in compound heterozygosity with R360C was associated with a severe complex neurological disorder including epilepsy, Parkinsonism, psychosis, visual and auditory hallucinations, gait ataxia and intellectual disability (48). Similarly, we engineered two different truncating alleles of mouse *Tbc1d24* (Fig. 1B) that reside on the same genetic background, one of which died perinatally, while pups homozygous for a frameshift allele have seizures and survived to P17–P20, indicating that a wild-type *Tbc1d24* gene likely has several different essential functions.

Here, we describe and characterize the first mouse model of human *TBC1D24* associated with early epileptic encephalopathy and provide a plausible mechanism to explain the abrupt onset of seizures at P15. There are many reports of seizures in humans associated with a great variety of mutations of *TBC1D24* suggesting that the S324Tfs*3 mouse could be used to validate (49) or possibly screen small molecule libraries for candidates that may generally prevent seizures and extend life. Future studies will also focus on uncovering the protein complexes and networks in which *TBC1D24* functions in the hippocampus and auditory system.

Materials and Methods

Animal care

Experiments with mice were conducted in accordance with the National Institutes of Health Guidelines for the Care and Use of Laboratory Animals. All experimental procedures were approved by the NIDCD Animal Care and Use Committee (ACUC) at the National Institutes of Health (protocol 1263-15 to T.B.F.). Experiments with mice were also approved by the University of Iowa ACUC (protocol 6031679 to B.B.).

Tbc1d24 mutant mice

Tbc1d24 mutant mice were obtained from the KOMP (Knockout Mouse Project) Repository at the Baylor College of Medicine. Unfortunately, both the *Tbc1d24*^{tm1a(EUCOMM)Hmgu} (RRID: MGI_4435698) and *Tbc1d24*^{tm1b(EUCOMM)Hmgu} (RRID: MGI_5692831) mutant mice were found to be homozygous lethal during embryogenesis and consequently not further studied. To obtain a homozygous pathogenic variant of *Tbc1d24* that was viable beyond P1, several different mutations of mouse *Tbc1d24* were engineered using CRISPR-mediated homologous recombination (HR) directly in C57BL/6J zygotes. For each of the two mutant alleles of *Tbc1d24* reported here, a few pairs of guide RNAs (gRNA) for SpCas9 (Protospacer adjacent motif (PAM) = NGG, where N is any nucleotide) were selected based on their relative positions to target codons and by their rankings using DESKGEN (www.deskgen.com), an online gRNA selection tool. gRNAs were synthesized using T7 *in vitro* transcription as described (50). To select the best pair of gRNAs that can efficiently direct the intended HR, gRNAs were further tested for their *in vitro* cleavage activities and for insertions and deletions (indel) mutagenesis efficiencies. For the *in vitro* cleavage assay, genomic PCR products containing the target sites of selected gRNAs were incubated with SpCas9 protein (New England Biolabs (NEB), Ipswich,

MA) following the manufacturer's protocol and analyzed on a 2% agarose gel stained with ethidium bromide (not shown). The gRNAs that failed to cleave target DNA fragments were eliminated, and the remaining gRNAs were further tested for their efficiencies to induce indels at target sites by a Surveyor nuclease assay in an immortalized mouse embryonic fibroblast cell line engineered to carry a tet-inducible Cas9 expression cassette as described (51). For the c.969_970delCT (p.S324Tfs*3) variant allele, the selected gRNA was mixed with SpCas9 protein (PNA Bio, Thousand Oaks, CA) along with a synthetic single-strand donor DNA oligo template for the c.969_970delCT (p.S324Tfs*3) variant allele as described above. Single-strand donor DNA oligo templates were designed to asymmetrically span the cleavage site and repair the DNA double-strand break introduced by the SpCas9 and gRNA (52).

Mixtures of each gRNA and purified SpCas9 protein were first incubated at room temperature for 15 min to associate gRNAs with Cas9 protein forming ribonuclear particles (RNPs) (53). The donor oligos were then added to the RNP preparation and microinjected into zygotes of C57BL/6J background as described (54). F0 founder mice were screened by PCR and sequencing for each mutation. In the process of generating a mutant mouse equivalent to the human D70Y allele (Fig. 1A), we obtained an on-target but unintended V67Sfs*4 allele, which was germline transmitted along with other alleles from a genetic mosaic F0 founder produced by CRISPR-Cas9-mediated genome editing. gRNAs used to create the V67Sfs*4 (*Tbc1d24*^{em1Tbf}, RRID: MGI_6195493) variant in mouse exon 3 and S324Tfs*3 variant (*Tbc1d24*^{em2Tbf}, RRID: MGI_6195494) located in mouse micro-exon 4 were 5'-GGCATAAGGTGTGACTGTG-3' and 5'-GAGACACTGAGAAACAGG-3', respectively. Donor oligo sequences of V67Sfs*4 and S324Tfs*3 were 5'-GAGCCACACCCTGCCGGGAAAGTGTACCAGCGCCTGATCCGGGACATCCCCTGCCGCACAGTCACACCTTATGCCAGCGTGTACAGTGACATTGT-3' (98 mer oligo) and 5'-caccactaacctc acctgtctctttttattttctctctctcctgtctcctgtctctctctgttctcagTGTCCATTTCTAAAAGgtaggtctg-3' (96 mer oligo), respectively. The nucleotide sequence in lower case is from introns flanking micro-exon 4.

Mice carrying the V67Sfs*4 allele were backcrossed with C57BL/6J for five generations and genotyped by Sanger sequencing the 403 bp amplified fragment generated by PCR using primers (5'-CAGCCTAGGACCTGCCTTG-3', 5'-TGGCAATACACAGGAGGATCT-3'). S324Tfs*3 mice were backcrossed with C57BL/6J for two generations and genotyped by PCR (5'-gaccgaaggaaggcatatc-3', 5'-ccaagcaccagcagatcata-3'). The resulting 347 bp amplicon was analyzed after Tsp45I restriction endonuclease digestion (NEB). The wild-type 347 bp amplicon was uncut by Tsp45I, while a mouse homozygous for the S324Tfs*3 allele generated a 345 bp amplicon and, when cut with Tsp45I, produced 106 bp and 239 bp restriction fragments.

Srrm3 and *Srrm4* mutant mice

Srrm3^{+/gt} mice were generated using an *Srrm3* gene-trapped embryonic stem cell clone obtained from the Texas A&M Institute for Genomic Medicine. Litters of *Srrm3*^{+/gt} breeding pairs were genotyped using DNA extracted from tail snips and conventional PCR. Primers to detect the *Srrm3*^{gt} allele were Fw: 5'-CGTACCATGCATGTGGAGGAC-3'; Rv: 5'-CCAATAAACCCCTCTTG CAGTTGC-3'; primers to detect the *Srrm3*^{WT} allele were Fw: 5'-CGTACCATGCATGTGGAGGAC-3'; Rv: 5'-AGACGTGTTGGGAGAATGACTAG-3'. qRT-PCR analysis of brain RNA samples revealed that *Srrm3* expression was 158.3 ± 26.76 (mean ± SEM)-fold lower in *Srrm3*^{gt/gt} mice than in wild-type mice at P16

($n = 3$ mice per group; Fw and Rv qRT-PCR primers for *Srrm3*: 5'-TCCAGCAGCTCTGCATCGCC-3' and 5'-AGTCTGCTCTTTTTGGC GCTC-3'; Fw and Rv qRT-PCR primers for the reference transcript *Heatr3*: 5'-CACACTTGACACTCTGAAGACC-3' and 5'-TCCAGAGCCTCGCTGTAC-3'). The *Srrm4*^{bu/bv} mouse line was described previously (33,55).

Alternative splicing of the *Tbc1d24* micro-exon

RNA was isolated from E14.5, P1, P7, P16 and P30 C57BL/6J wild-type brains using a Direct-zol RNA MiniPrep kit (Zymo Research, Irvine, CA). Transcripts of *Tbc1d24* were PCR amplified from cDNA synthesized using a SuperScript III First-Strand Synthesis system (Thermo Fisher Scientific, Waltham, MA). Primers used to specifically amplify cDNAs from mouse *Tbc1d24* were Fw: 5'-CTGAGGCAGAAGGGTATAACTG-3'; Rv: 5'-GGACCAAATGTCTCTCATCTCC-3'. The sequence of the Fw primer is from exon 3 and the primer Rv is complementary to the sequence in exon 5. PCR products were subcloned into pCR4-TOPO TA vector (Thermo Fisher Scientific), and Sanger sequenced.

For quantitative RT-PCR (qRT-PCR), RNA was isolated from the neocortex of wild-type mice at E14.5, E18.5 and P16 using TRIzol Reagent (Thermo Fisher Scientific). Isolated RNA was incubated with DNase and further purified on a column from an RNeasy Mini Kit (Qiagen, Germantown, MD), following the manufacturer's instructions. RNA samples were reverse-transcribed using SuperScript IV Reverse Transcriptase and Random Primers (Thermo Fisher Scientific). The cDNA products were analyzed for the incorporation of exon 4 into the *Tbc1d24* mRNA by qRT-PCR. We designed primers to detect micro-exon 4-containing *Tbc1d24* transcripts (Fw: 5'-CTGTCAAACAGAAGAGTGTCTC-3'; Rv: 5'-CTCCTTACAGCTGACAATCTC-3') and to detect total mRNA levels of *Tbc1d24* (Fw: 5'-GAAGGAGATGAGAGACATTTGG-3'; Rv: 5'-CTGGAAATAGAACCTGCTTAGG-3').

For the RT-PCR analysis of *Srrm4*^{bu/bv} (Bronx waltzer) (33), *Srrm3*^{gt/gt} mutant mice (Y. Nakano and B. Banfi, manuscript in preparation) and wild-type, RNA was isolated from brain cortex at P16 and the RNA samples were reverse transcribed using the same protocols as above. Primers used to amplify cDNAs from mouse *Tbc1d24* were Fw: 5'-GAAAGCACTGAGGCAGAAGGG-3'; Rv: 5'-TGAGTGAAGTTCTCTGCATGG-3'.

For RNA-seq analyses, whole cochleae, including spiral ganglion tissues, were dissected from three C57BL/6 mice at P49. The cochleae were placed in TT1 tissue tubes (Covaris, Woburn, MA), snap frozen in liquid nitrogen, then crushed using a Covaris CP02 CryoPREP Impactor. The crushed tissue was immediately submerged in TRIzol Reagent (Thermo Fisher Scientific), and RNA was extracted using the manufacturer's recommended protocol. RNA was prepared for sequencing on an Illumina HiSeq instrument using TruSeq preparation kit (Illumina, San Diego, CA). The 90 × 90 paired-end reads were mapped to the mouse genome (Gencode GRCm38.vM11) using the STAR aligner (56). RNA-seq data for E16.5 and P0 cochleae were derived from Ushakov and co-authors (57) and downloaded from GEO (GSE97270) (<https://www.ncbi.nlm.nih.gov/geo/>).

Cloning procedures

The *Tbc1d24* minigene was generated by subcloning the PCR-amplified micro-exon 4 and adjacent ~650 bp intronic sequence of mouse *Tbc1d24* (PCR primers: 5'-AACAAATCGATTAACAAGACA AGGAAGCTGGG-3' and 5'-TGGATACTAGTAGAAACCAGGACAAAT

GAAGTAAG-3') between two constitutively spliced exons in the pET-01 vector (Mobictec, Göttingen, Germany). The coding regions of *Srrm3*, *Nova1* and *Rbfox1* were amplified by RT-PCR from mouse brain RNA and subcloned into the pcDNA3.1 expression vector (*Srrm3* primers 5'-ACTAGTGCCACCATGTCTCCACCCTGAA CAAC-3' and 5'-GATATCTCGAGCTTAGAAGCCCCCACTCTCAG; *Nova1* primers 5'-TTTTTAGCTAGCCACCATGATGGCGGCAGCTCC CATTTC-3' and 5'-ATAGTTTAGCGGCCGCTCAACCCACTTTCTGAG GATTG-3'; *Rbfox1* primers 5'-ATTAAAGCTAGCCACCATGAATTG TGAAAGAGAGCAGC and 5'-AATTAAAGCGGCCGCATTTAATATG GAGCAAAACGGTTG-3'). The SRRM4-encoding expression plasmid was described previously (33).

Splicing assays in transfected HEK293 cells

HEK293 cells were obtained from the American Type Culture Collection and were grown in Dulbecco's Modified Eagle Medium/Nutrient Mixture F-12 (F-12 from Corning) supplemented with 10% fetal bovine serum (Atlanta Biologicals, Lawrenceville, GA), penicillin (100 units/ml; Thermo Fisher Scientific) and streptomycin (100 µg/ml; Thermo Fisher Scientific) at 37°C in the presence of 5% CO₂. HEK293 cells were co-transfected with the *Tbc1d24* minigene and an empty expression vector (pcDNA3.1), a NOVA1-encoding plasmid, an SRRM3-encoding plasmid, an SRRM4-encoding plasmid or an RBOX1-encoding plasmid using Lipofectamine LTX and PLUS reagent (Thermo Fisher Scientific). RNA was isolated from the cells 24 h after transfection using RNeasy Mini Kit (Qiagen). The splicing of minigene-encoded transcripts was tested by RT-PCR using the following primers: 5'-CACTTGGTGAAGCTCTCTACC-3' and 5'-CCACTCCAGTGCCAAGGTC-3'. RT-PCR products were separated by polyacrylamide gel electrophoresis. Band intensities in gel images were quantified using the ImageJ software. Percent spliced in (PSI) was calculated by dividing the band intensity of the longer (i.e. micro-exon 4-containing) splice form by the summed band intensities of the shorter and longer splice forms.

Natural history, open-field recordings and data analyses

Mice were maintained on a 12 h light and 12 h dark cycle at 70–74°F with humidity ranging from 30–65%. Homozygous S324Tfs*3 mice (9 males and 17 females), heterozygous S324Tfs*3 mice (27 males and 31 females) and wild-type (9 males and 16 females) littermates were monitored for survival from P0 to P180. Animals were genotyped using PCR to confirm sex if pups died before weaning. Genomic DNA from a male pup used as a template produced 302 bp and 331 bp amplicons, while genomic DNA from a female pup as a template generated only a 331 bp amplicon with primers 5'-CTGAAGCTTTGGCTTTGAG-3' and 5'-CCACTGCCAAATCTTTGG-3' (58).

Seizuring in a mouse was defined as either serial abnormal movements, such as wild running (uncontrollable movement at high velocity), convulsions (tonic-clonic seizure with muscle rigidity and jerking movements) or postictal state (26–28). Severity of seizure was scored using the Racine scale (59,60): stage 1, chewing or excess secretion; stage 2, whole-body twitching/tremors; stage 3, unilateral forelimb clonus or paralysis; stage 4, bilateral forelimb clonus; stage 5, severe convulsions. In the open-field test, homozygous S324Tfs*3 (4 males and 5 females), heterozygous S324Tfs*3 (5 males and

5 females) and wild-type (4 males and 4 females) littermates were evaluated longitudinally at P5, P7, P9, P11, P13, P15, P16 and P17 between 9 am and 1 pm. Since neonatal pups were separated from their mother during open-field tests, recordings were limited to only 30 min. The observer was blinded to the genotypes of the mice during recordings.

After adaptation in a quiet testing room for ~10 min, individual mice were placed in a Plexiglass chamber (17.5 × 31.8 × 14.5 cm). The position of each mouse was recorded using an overhead camera at 30 frames per s (EverFocus EQ700, New Taipei, China) for 30 min. Post hoc position analyses were performed with TopScan (Clever Systems, Inc., Reston, VA), which tracked and logged the x and y coordinates of the center of the body for each frame of the video. The trajectories of mouse movements including those in time-lapse movies were plotted using Python (<https://www.python.org/>) with Matplotlib (<https://matplotlib.org/>). The speed of the mouse is indicated by the color of each point, which was mapped to a jet colormap in the range of 0–15 cm/s. Speeds of >15 cm/s were clipped to this maximum value.

The distance (cm) traveled between successive video frames was used to calculate frame-by-frame velocity. The distance from the previously recorded position to the current position was divided by the video frame rate. Recordings indicated that the wild-running seizures of homozygous S324Tfs*3 mice persisted for as long as 1 min. Therefore, a sliding 1 min time bin was used to detect wild-running that comprised the first phase of a mouse seizure. This bin was advanced frame by frame to provide a unique set of video frames and velocity measurements. This isolated the within-session 1 min time interval with the highest velocity. The numerically flagged seizure detection was validated by manual observation of each video acquired at P17. Mean 1 min distance traveled by wild-type and heterozygous mice was determined using the entire 30 min recording. Mean 1 min distances traveled in the 'normal state' of homozygous S324Tfs*3 mice were collected using the segment from the beginning of the recording to the time point 1 min before wild-running. In homozygous S324Tfs*3 mice with seizures, the start and end time of the highest velocity bin (wild-running), the start and end time of the 1 min period prior to this bin (pre-seizure) and the bin 1 min following the wild-running (convulsions and postictal state) were compared using a one-way repeated measures ANOVA with Tukey's post hoc analysis.

ABR, DPOAE and VsEP measurements

Auditory testing of homozygous S324Tfs*3 ($n = 4$), heterozygous S324Tfs*3 ($n = 4$) and wild-type ($n = 3$) littermates at P17 was completed in the Mouse Auditory Testing Core facility, NIDCD/NIH as previously described (61). Briefly, mice were anesthetized by an intraperitoneal (IP) injection of a combination of 56 mg/kg body weight of ketamine (VetOne; MWI Animal Health, Boise, ID) and 0.375 mg/kg body weight of dexdomitor (Putney Inc., Portland, ME). Puralube eye ointment was applied to protect corneas once adequate anesthesia was achieved. Both ABRs and DPOAEs were measured in the right ear using Tucker-Davis Technologies (TDT, Alachua, FL) hardware (RZ6 Multi I/O processor, MF-1 speakers, TDT) and software (BioSigRz, v. 5.7.2, TDT).

P16 homozygous S324Tfs*3 ($n = 4$), heterozygous S324Tfs*3 ($n = 4$) and wild-type ($n = 3$) littermates were anesthetized as described above prior to measuring VsEPs (62). Subcutaneous electrodes were placed at the nuchal crest (non-inverting), at the left ear (inverting) and at the right hip (ground). Mice

were placed supine on a stationary heating pad held at 37°C to maintain body temperature. The head was placed in a non-invasive head clip lined with soft foam weather stripping with the nose aimed upward. The stimuli were rectangular jerk pulses (1.0 g/ms, 2 ms duration) delivered at a rate of 17/s. Linear acceleration ramps were applied to an RMX850 power amplifier (QSC, Costa Mesa, CA) that drove a mechanical shaker (Labworks, Inc., Costa Mesa, CA) coupled to the head clip via a custom metal plate to deliver the stimulus. The resultant translational head motion was in the naso-occipital axis, stimulating the saccule and utricle of the mouse. The stimulus was calibrated and monitored throughout testing by routing the output of a calibrated accelerometer (VibraMetrics Model 1018; Princeton Junction, NJ) mounted to the same plate that held the head clip to a custom-built differentiator to convert it to jerk [(g/ms, where 1 g = 9.8 m/s²), described in Jones et al. (62)]. The stimulus level was expressed in dB relative to 1 g/ms (dB re: 1 g/ms). VsEP responses were measured from the left side using TDT hardware (RZ6 Multi I/O processor, Medusa preamplifier and a headstage) and software (BioSigRz, v. 5.7.2). The raw signal from the scalp was amplified (20×), filtered (300–3000 Hz) and digitized (25 kHz). Each final VsEP response was obtained by averaging responses to 256 positive polarity and to 256 inverted stimuli. Two averaged responses were recorded for each intensity level. To determine threshold, stimuli were presented between +6 dB to –18 dB, descending in 3 dB steps. Threshold was defined as the intensity halfway between the lowest stimulus at which a measurable and repeatable response was observed and the next lowest intensity level. Latency and amplitude measures of peaks P1 and P2 were evaluated offline for the highest intensity level (+6 dB).

Brain histopathology

Blinded to genotype, 7 homozygous S324Tfs*3 mice (2 males and 2 females at P14 and 2 males and 1 female at P17) and 5 wild-type littermate controls (1 male and 1 female at P14 and 2 males and 1 female at P17) were euthanized with CO₂. The brains of these mice were removed and fixed in 10% buffered formalin, processed, embedded in paraffin and 5 μm sections were prepared and stained with hematoxylin and eosin. Slides were evaluated by M.F.S. using an Olympus BX41 light microscope (Olympus, Tokyo, Japan).

In situ hybridization using an RNAscope probe

In situ hybridization to detect transcripts of *Tbc1d24* was performed using an RNAscope Probe-Mm-Tbc1d24 (target region: 839–1739 nucleotides, NM_001163847.1), available from Advanced Cell Diagnostics (Newark, CA), and a negative control RNAscope Probe-DapB. Brains from C57BL/6J wild-type mice at P30, from homozygous S324Tfs*3 mice at P17 and wild-type littermate controls and cochleae from C57BL/6J wild-type at P3 were used. Mice were deeply anesthetized with an IP injection of a solution of ketamine (120 mg/kg) and xylazine (25 mg/kg) (AnaSed, Akorn, Lake Forest, IL), perfused transcardially at 4 ml/min with 15 ml of 1× phosphate buffered saline (PBS) and then with 40 ml of 4% paraformaldehyde (PFA; Electron Microscopy Sciences, Hatfield, PA) in 1× PBS using a peristaltic pump (Pharmacia, Uppsala, Sweden). The brain was removed and stored in 4% PFA at 4°C for 24 h. Brains were then cryopreserved in 15 and 30% sucrose at 4°C overnight. Each brain was embedded and frozen in Super Cryoembedding

Medium (Section-lab, Hiroshima, Japan). Frozen tissues were sagittally oriented and sectioned (10 μm thickness) with a cryostat microtome (CM3050S; Leica, Vienna, Austria). An RNAscope 2.5 HD assay-RED was conducted to visualize single RNA molecules with RNAscope Probe-Mm-Tbc1d24 (Advanced Cell Diagnostics). Images were taken using a Nikon Eclipse 90i microscope with 10 \times and 20 \times objectives with tile scanning (Nikon, Tokyo, Japan).

Antibody validation and immunohistochemistry

Brains of homozygous V67Sfs*4 mice and wild-type littermate controls at E18.5 were dissected, and fixed overnight with 4% PFA in 1 \times PBS at 4°C. Cryosections were prepared as described above and post-fixed with 1.5% PFA, permeabilized with 0.1% Triton X-100 and blocked with 2% BSA (bovine serum albumin) and 5% goat serum in 1 \times PBS. Samples were incubated with a 1:400 dilution of primary antibody against TBC1D24 antibody (NBP1-82925, RRID: AB_11061868; Novus Biologicals, Littleton, CO) and 1:1000 dilution of Neurofilament-NF-H antibody (MAB5448, RRID: AB_11214466; MilliporeSigma, Burlington, MA), washed in 1 \times PBS and stained with Alexa Fluor 488, anti-rabbit IgG secondary antibody and Alexa Fluor 568, anti-rat IgG secondary antibody (Thermo Fisher Scientific). After washing in 1 \times PBS, samples were mounted in ProLong Gold Antifade Mountant (Thermo Fisher Scientific). Samples were imaged with 40 \times , 1.4 NA tile scanning using an LSM780 confocal microscope (Zeiss, Thornwood, NY). P17 wild-type and homozygous S324Tfs*3 littermate mouse inner ear samples were fixed with 4% PFA in 1 \times PBS at 4°C overnight, permeabilized in 0.5% Triton X-100 for 15 min at room temperature and stained with rhodamine-phalloidin (Thermo Fisher Scientific) at 1:100 dilution in 1 \times PBS for 20 min at room temperature. After several washes in 1 \times PBS, samples were mounted using ProLong Gold Antifade Mountant (Thermo Fisher Scientific) and examined using an LSM780 confocal microscope (Zeiss) equipped with 63 \times , 1.4 NA objective.

Immunoblotting

Brain lysates from homozygous V67Sfs*4 mice and wild-type littermate controls at E18.5 and homozygous S324Tfs*3 mice and wild-type littermate controls at P1 were prepared in RIPA buffer with Halt Protease Inhibitor Cocktail (Thermo Fisher Scientific). Protein concentration in lysates was measured with Pierce 660 nm Protein Assay Reagent (Thermo Fisher Scientific) using a NanoDrop spectrophotometer (Thermo Fisher Scientific). A total of 20 mg of each protein were size-separated on a 4–20% gradient SDS-PAGE gel (Bio-Rad, Hercules, CA), transferred to a membrane using a Bio-Rad Trans-Blot Turbo Mini PVDF Transfer Pack and probed with the following antibodies using an iBind western system (Thermo Fisher Scientific): TBC1D24 antibody (NBP1-82925; 1:1000 dilution, Novus Biologicals), α -tubulin antibody (T9026; 1: 40 000 dilution, Sigma-Aldrich), anti-rabbit IgG-peroxidase antibody (A0545; 1:8000 dilution, Sigma-Aldrich) and anti-mouse IgG-peroxidase antibody (A9044; 1:8000 dilution, Sigma-Aldrich).

Immuno-TEM

For post-embedding immunogold [details in (63)], mice were perfused with 4% PFA with 0.5% glutaraldehyde. Slices of the

hippocampus were cryoprotected and frozen in a Leica CPC and then processed for freeze-substitution in Lowicryl HM-20 resin in a Leica AFS. Thin sections were incubated in 0.1% sodium borohydride plus 50 mM glycine in Tris-buffered saline plus 0.1% Triton X-100 (TBST). Sections were incubated first in 10% normal goat serum, and then overnight in the primary antibody, followed by incubation for 1 h with 10 nm immunogold (1:40 dilution) in 1% NGS (normal goat serum)/TBST + 0.5% polyethylene glycol 20 000 (Fluka Chemie AG, Buchs, Switzerland). Finally, the sections were stained with 0.1% uranyl acetate and 0.03% lead citrate (Electron Microscopy Sciences).

Rabbit anti-TBC1D24 antibody (NBP1-82925, Novus Biologicals) was used on hippocampus sections from two 8-week-old male wild-type C57BL/6 mice (64). Immunogold labeling and imaging with the anti-TBC1D24 antibody were repeated two and three times for the two mice. Images were taken from the CA1 stratum radiatum–pyramidale and from the CA3 stratum lucidum–pyramidale. Control immunogold labeling of sections lacking just the primary antibody produced only rare gold particles.

Ex vivo MRI sample, MRI acquisition and qualitative analysis

Four homozygous S324Tfs*3 mice and four wild-type mice at P17 were examined using ex vivo MRI. Tissue from each mouse was fixed with 4% PFA in 1 \times PBS containing 1 $\mu\text{mol/l}$ of gadopentetate dimeglumine (Magnevist; Bayer HealthCare Pharmaceuticals Inc., Whippany, NJ) via cardiac perfusion. The mouse head was removed and placed in the same fixative for 24 h at 4°C, and then transferred to 1 \times PBS solution with 0.1% sodium azide. Prior to scanning, the skin, eyes, mandible and any remaining musculature were removed from each specimen. The brain remained inside the cranium for scanning to preserve the brain anatomy.

MRI acquisition was performed on a 14T Bruker microimaging system with a 10 mm linear radio frequency coil. A T2-weighted image was acquired using a multislice multiecho pulse sequence with 100 μm isotropic resolution and a matrix size of 160 \times 84 \times 80 and with TE (echo time)/TR (repetition time) = 30/3000, nex = 1. Optimized automatic registration (MIPAV v7.2.0, <https://mipav.cit.nih.gov>) was used to rigidly register the raw images into Waxholm space template for visual inspection (65).

Supplementary Material

Supplementary Material is available at HMG online.

Acknowledgements

We are grateful for Lin Lin and Dax Hoffman for mouse tissue, and we also thank Dennis Drayna, Michael Hoa, Isabelle Roux, Cristina Fenollar-Ferrer, Elizabeth Bernhard, James McGehee, Patrick Diers, Ayesha Imtiaz, Melanie Barzik, Joseph Duda and Alexander Callahan. The behavioral work was conducted in the National Institute of Mental Health Rodent Behavioral Core. This work utilized the computational resources of the NIH High performance computation Biowulf cluster (<http://hpc.nih.gov>). The authors also thank Sherri Jones, Timothy Jones and Sarath Vijayakumar of the University of Nebraska-Lincoln and John Kakareka, Thomas Pohida, Jessica Crouch and Connor Schultz from the Signal Processing and Instrumentation Section of the

Computational Bioscience and Engineering Laboratory at the National Institutes of Health for assistance with development of the VsEP unit.

Conflict of Interest statement. None declared.

Funding

National Institute of Mental Health (ZIA MH002951 and ZIC MH002952 to Y.C.); National Institute on Deafness and Other Communication Disorders (DC000080 to T.S.F., DC000081 to R.S.P. and Y.-X.W., DC000086 to R.J.M., R01DC014953 to B.B. and DC000039 to T.B.F.); National Institute of Biomedical Imaging and Bioengineering (EB000088-02 to C.P.).

References

- Fukuda, M. (2011) TBC proteins: GAPs for mammalian small GTPase Rab. *Biosci. Rep.*, **31**, 159–168.
- Fischer, B., Lüthy, K., Paesmans, J., De Koninck, C., Maes, I., Swerts, J., Kuenen, S., Uytterhoeven, V., Verstreken, P. and Versées, W. (2016) Skywalker-TBC1D24 has a lipid-binding pocket mutated in epilepsy and required for synaptic function. *Nat. Struct. Mol. Biol.*, **23**, 965–973.
- Campeau, P.M., Kasperaviciute, D., Lu, J.T., Burrage, L.C., Kim, C., Hori, M., Powell, B.R., Stewart, F., Félix, T.M., van den Ende, J. et al. (2014) The genetic basis of DOORS syndrome: an exome-sequencing study. *Lancet Neurol.*, **13**, 44–58.
- Corbett, M.A., Bahlo, M., Jolly, L., Afawi, Z., Gardner, A.E., Oliver, K.L., Tan, S., Coffey, A., Mulley, J.C., Dibbens, L.M. et al. (2010) A focal epilepsy and intellectual disability syndrome is due to a mutation in TBC1D24. *Am. J. Hum. Genet.*, **87**, 371–375.
- Rehman, A.U., Santos-Cortez, R.L., Morell, R.J., Drummond, M.C., Ito, T., Lee, K., Khan, A.A., Basra, M.A., Wasif, N., Ayub, M. et al. (2014) Mutations in TBC1D24, a gene associated with epilepsy, also cause nonsyndromic deafness DFN86. *Am. J. Hum. Genet.*, **94**, 144–152.
- Frasa, M.A., Koessmeier, K.T., Ahmadian, M.R. and Braga, V.M. (2012) Illuminating the functional and structural repertoire of human TBC/RABGAPs. *Nat. Rev. Mol. Cell Biol.*, **13**, 67–73.
- Ivanova, E.L., Mau-Them, F.T., Riazuddin, S., Kahrizi, K., Laugel, V., Schaefer, E., de Saint Martin, A., Runge, K., Iqbal, Z., Spitz, M.A. et al. (2017) Homozygous truncating variants in TBC1D23 cause pontocerebellar hypoplasia and alter cortical development. *Am. J. Hum. Genet.*, **101**, 428–440.
- Azaiez, H., Booth, K.T., Bu, F., Huygen, P., Shibata, S.B., Shearer, A.E., Kolbe, D., Meyer, N., Black-Ziegelbein, E.A. and Smith, R.J. (2014) TBC1D24 mutation causes autosomal-dominant nonsyndromic hearing loss. *Hum. Mutat.*, **35**, 819–823.
- Zhang, L., Hu, L., Chai, Y., Pang, X., Yang, T. and Wu, H. (2014) A dominant mutation in the stereocilia-expressing gene TBC1D24 is a probable cause for nonsyndromic hearing impairment. *Hum. Mutat.*, **35**, 814–818.
- Falace, A., Filipello, F., La Padula, V., Vanni, N., Madia, F., De Pietri Tonelli, D., de Falco, F.A., Striano, P., Dagna Bricarelli, F., Minetti, C. et al. (2010) TBC1D24, an ARF6-interacting protein, is mutated in familial infantile myoclonic epilepsy. *Am. J. Hum. Genet.*, **87**, 365–370.
- Muona, M., Berkovic, S.F., Dibbens, L.M., Oliver, K.L., Maljevic, S., Bayly, M.A., Joensuu, T., Canafoglia, L., Franceschetti, S., Michelucci, R. et al. (2015) A recurrent de novo mutation in KCNC1 causes progressive myoclonus epilepsy. *Nat. Genet.*, **47**, 39–46.
- Mucha, B.E., Banka, S., Ajeawung, N.F., Molidperee, S., Chen, G.G., Koenig, M.K., Adejumo, R.B., Till, M., Harbord, M., Perrier, R. et al. (2018) A new microdeletion syndrome involving TBC1D24, ATP6V0C, and PDPK1 causes epilepsy, microcephaly, and developmental delay. *Genet. Med.*, doi:10.1038/s41436-018-0290-3.
- Finelli, M.J. and Oliver, P.L. (2017) TLDc proteins: new players in the oxidative stress response and neurological disease. *Mamm. Genome*, **28**, 395–406.
- Albert, S., Will, E. and Gallwitz, D. (1999) Identification of the catalytic domains and their functionally critical arginine residues of two yeast GTPase-activating proteins specific for Ypt/Rab transport GTPases. *EMBO J.*, **18**, 5216–5225.
- Yoshimura, S., Egerer, J., Fuchs, E., Haas, A.K. and Barr, F.A. (2007) Functional dissection of Rab GTPases involved in primary cilium formation. *J. Cell Biol.*, **178**, 363–369.
- Pan, X., Eathiraj, S., Munson, M. and Lambright, D.G. (2006) TBC-domain GAPs for Rab GTPases accelerate GTP hydrolysis by a dual-finger mechanism. *Nature*, **442**, 303–306.
- Uytterhoeven, V., Kuenen, S., Kasprovicz, J., Miskiewicz, K. and Verstreken, P. (2011) Loss of skywalker reveals synaptic endosomes as sorting stations for synaptic vesicle proteins. *Cell*, **145**, 117–132.
- Balestrini, S., Milh, M., Castiglioni, C., Lüthy, K., Finelli, M.J., Verstreken, P., Cardon, A., Stražišar, B.G., Holder, J.L. Jr., Lesca, G. et al. (2016) TBC1D24 genotype–phenotype correlation: epilepsies and other neurologic features. *Neurology*, **87**, 77–85.
- Kammenga, J.E. (2017) The background puzzle: how identical mutations in the same gene lead to different disease symptoms. *FEBS J.*, **284**, 3362–3373.
- Yousaf, R., Ahmed, Z.M., Giese, A.P., Morell, R.J., Lagziel, A., Dabdoub, A., Wilcox, E.R., Riazuddin, S., Friedman, T.B. and Riazuddin, S. (2018) Modifier variant of METTL13 suppresses human GAB1-associated profound deafness. *J. Clin. Invest.*, **128**, 1509–1522.
- Zotenko, E., Mestre, J., O’Leary, D.P. and Przytycka, T.M. (2008) Why do hubs in the yeast protein interaction network tend to be essential: reexamining the connection between the network topology and essentiality. *PLoS Comput. Biol.*, **4**, e1000140.
- Falace, A., Buhler, E., Fadda, M., Watrin, F., Lippiello, P., Pallesi-Pocachard, E., Baldelli, P., Benfenati, F., Zara, F., Represa, A. et al. (2014) TBC1D24 regulates neuronal migration and maturation through modulation of the ARF6-dependent pathway. *Proc. Natl. Acad. Sci. U. S. A.*, **111**, 2337–2342.
- Yoon, J., Hwang, Y.S., Lee, M., Sun, J., Cho, H.J., Knapik, L. and Daar, I.O. (2018) TBC1d24-ephrinB2 interaction regulates contact inhibition of locomotion in neural crest cell migration. *Nat. Commun.*, **9**, 3491.
- Güven, A. and Tolun, A. (2013) TBC1D24 truncating mutation resulting in severe neurodegeneration. *J. Med. Genet.*, **50**, 199–202.
- Duru, N., Iseri, S.A., Selcuk, N. and Tolun, A. (2010) Early-onset progressive myoclonic epilepsy with dystonia mapping to 16pter-p13.3. *J. Neurogenet.*, **24**, 207–215.
- Holmes, G.L. and Noebels, J.L. (2016) *Epilepsy: The Biology of a Spectrum Disorder*. Cold Spring Harbor Laboratory Press, Cold Spring Harbor, NY.
- N’Gouemo, P. and Faingold, C.L. (1998) Periaqueductal gray neurons exhibit increased responsiveness associated with

- audiogenic seizures in the genetically epilepsy-prone rat. *Neuroscience*, **84**, 619–625.
28. Ross, K.C. and Coleman, J.R. (2000) Developmental and genetic audiogenic seizure models: behavior and biological substrates. *Neurosci. Biobehav. Rev.*, **24**, 639–653.
 29. Rehman, A.U., Bird, J.E., Faridi, R., Shahzad, M., Shah, S., Lee, K., Khan, S.N., Imtiaz, A., Ahmed, Z.M., Riazuddin, S. et al. (2016) Mutational spectrum of MYO15A and the molecular mechanisms of DFNB3 human deafness. *Hum. Mutat.*, **37**, 991–1003.
 30. Lykke-Andersen, S. and Jensen, T.H. (2015) Nonsense-mediated mRNA decay: an intricate machinery that shapes transcriptomes. *Nat. Rev. Mol. Cell Biol.*, **16**, 665–677.
 31. Petralia, R.S., Wang, Y.X., Mattson, M.P. and Yao, P.J. (2018) Invaginating structures in mammalian synapses. *Front. Synaptic Neurosci.*, **10**, 4.
 32. Milosevic, I. (2018) Revisiting the role of clathrin-mediated endocytosis in synaptic vesicle recycling. *Front. Cell. Neurosci.*, **12**, 27.
 33. Nakano, Y., Jahan, I., Bonde, G., Sun, X., Hildebrand, M.S., Engelhardt, J.F., Smith, R.J., Cornell, R.A., Fritzsche, B. and Bánfi, B. (2012) A mutation in the *Srrm4* gene causes alternative splicing defects and deafness in the Bronx waltzer mouse. *PLoS Genet.*, **8**, e1002966.
 34. Anderson, K.R., Haeussler, M., Watanabe, C., Janakiraman, V., Lund, J., Modrusan, Z., Stinson, J., Bei, Q., Buechler, A., Yu, C. et al. (2018) CRISPR off-target analysis in genetically engineered rats and mice. *Nat. Methods*, **15**, 512–514.
 35. Kosicki, M., Tomberg, K. and Bradley, A. (2018) Repair of double-strand breaks induced by CRISPR-Cas9 leads to large deletions and complex rearrangements. *Nat. Biotechnol.*, **36**, 765–771.
 36. Raj, B. and Blencowe, B.J. (2015) Alternative splicing in the mammalian nervous system: recent insights into mechanisms and functional roles. *Neuron*, **87**, 14–27.
 37. Fiol, C.J., Wang, A., Roeske, R.W. and Roach, P.J. (1990) Ordered multisite protein phosphorylation. Analysis of glycogen synthase kinase 3 action using model peptide substrates. *J. Biol. Chem.*, **265**, 6061–6065.
 38. Pearson, R.B. and Kemp, B.E. (1991) Protein kinase phosphorylation site sequences and consensus specificity motifs: tabulations. *Methods Enzymol.*, **200**, 62–81.
 39. Barker-Haliski, M. and White, H.S. (2015) Glutamatergic mechanisms associated with seizures and epilepsy. *Cold Spring Harb. Perspect. Med.*, **5**, a022863.
 40. Devinsky, O., Vezzani, A., O'Brien, T.J., Jette, N., Scheffer, I.E., de Curtis, M. and Perucca, P. (2018) Epilepsy. *Nat. Rev. Dis. Primers*, **4**, 18024.
 41. Sutula, T., He, X.X., Cavazos, J. and Scott, G. (1988) Synaptic reorganization in the hippocampus induced by abnormal functional activity. *Science*, **239**, 1147–1150.
 42. Schwartzkroin, P.A. and Knowles, W.D. (1984) Intracellular study of human epileptic cortex: in vitro maintenance of epileptiform activity. *Science*, **223**, 709–712.
 43. Blümcke, I., Thom, M. and Wiestler, O.D. (2002) Ammon's horn sclerosis: a maldevelopmental disorder associated with temporal lobe epilepsy. *Brain Pathol.*, **12**, 199–211.
 44. de Lanerolle, N.C. and Lee, T.S. (2005) New facets of the neuropathology and molecular profile of human temporal lobe epilepsy. *Epilepsy Behav.*, **7**, 190–203.
 45. de Falco, F.A., Majello, L., Santangelo, R., Stabile, M., Bricarelli, F.D. and Zara, F. (2001) Familial infantile myoclonic epilepsy: clinical features in a large kindred with autosomal recessive inheritance. *Epilepsia*, **42**, 1541–1548.
 46. Milh, M., Falace, A., Villeneuve, N., Vanni, N., Cacciagli, P., Assereto, S., Nabbout, R., Benfenati, F., Zara, F., Chabrol, B. et al. (2013) Novel compound heterozygous mutations in *TBC1D24* cause familial malignant migrating partial seizures of infancy. *Hum. Mutat.*, **34**, 869–872.
 47. Finelli, M.J., Aprile, D., Castroflorio, E., Jeans, A., Moschetta, M., Chessum, L., Degiacomi, M.T., Grasegger, J., Lupien-Meilleur, A., Bassett, A. et al. (2018) The epilepsy-associated protein *TBC1D24* is required for normal development, survival and vesicle trafficking in mammalian neurons. *Hum. Mol. Genet.*, doi: [10.1093/hmg/ddy370](https://doi.org/10.1093/hmg/ddy370).
 48. Banuelos, E., Ramsey, K., Belnap, N., Krishnan, M., Balak, C., Szelinger, S., Siniard, A.L., Russell, M., Richholt, R., De Both, M. et al. (2017) Case report: novel mutations in *TBC1D24* are associated with autosomal dominant tonic-clonic and myoclonic epilepsy and recessive Parkinsonism, psychosis, and intellectual disability. *F1000Res.*, **6**, 553.
 49. Löscher, W., Klitgaard, H., Twyman, R.E. and Schmidt, D. (2013) New avenues for anti-epileptic drug discovery and development. *Nat. Rev. Drug Discov.*, **12**, 757–776.
 50. Varshney, G.K., Pei, W., LaFave, M.C., Idol, J., Xu, L., Gallardo, V., Carrington, B., Bishop, K., Jones, M., Li, M. et al. (2015) High-throughput gene targeting and phenotyping in zebrafish using CRISPR/Cas9. *Genome Res.*, **25**, 1030–1042.
 51. Pilato, B., De Summa, S., Danza, K., Papadimitriou, S., Zaccagna, P., Paradiso, A. and Tommasi, S. (2012) DHPLC/SURVEYOR nuclease: a sensitive, rapid and affordable method to analyze *BRCA1* and *BRCA2* mutations in breast cancer families. *Mol. Biotechnol.*, **52**, 8–15.
 52. Richardson, C.D., Ray, G.J., DeWitt, M.A., Curie, G.L. and Corn, J.E. (2016) Enhancing homology-directed genome editing by catalytically active and inactive CRISPR-Cas9 using asymmetric donor DNA. *Nat. Biotechnol.*, **34**, 339–344.
 53. Kim, S., Kim, D., Cho, S.W., Kim, J. and Kim, J.S. (2014) Highly efficient RNA-guided genome editing in human cells via delivery of purified Cas9 ribonucleoproteins. *Genome Res.*, **24**, 1012–1019.
 54. Wang, H., Yang, H., Shivalila, C.S., Dawlaty, M.M., Cheng, A.W., Zhang, F. and Jaenisch, R. (2013) One-step generation of mice carrying mutations in multiple genes by CRISPR/Cas-mediated genome engineering. *Cell*, **153**, 910–918.
 55. Nakano, Y., Kelly, M.C., Rehman, A.U., Boger, E.T., Morell, R.J., Kelley, M.W., Friedman, T.B. and Bánfi, B. (2018) Defects in the alternative splicing-dependent regulation of *REST* cause deafness. *Cell*, **174**, 536.e21–548.e21.
 56. Dobin, A., Davis, C.A., Schlesinger, F., Drenkow, J., Zaleski, C., Jha, S., Batut, P., Chaisson, M. and Gingeras, T.R. (2013) STAR: ultrafast universal RNA-seq aligner. *Bioinformatics*, **29**, 15–21.
 57. Ushakov, K., Koffler-Brill, T., Rom, A., Perl, K., Ulitsky, I. and Avraham, K.B. (2017) Genome-wide identification and expression profiling of long non-coding RNAs in auditory and vestibular systems. *Sci. Rep.*, **7**, 8637.
 58. Clapcote, S.J. and Roder, J.C. (2005) Simplex PCR assay for sex determination in mice. *Biotechniques*, **38**, 702, 704, 706.
 59. Racine, R.J. (1972) Modification of seizure activity by electrical stimulation. II. Motor seizure. *Electroencephalogr. Clin. Neurophysiol.*, **32**, 281–294.
 60. Reddy, D.S. and Kuruba, R. (2013) Experimental models of status epilepticus and neuronal injury for evaluation of therapeutic interventions. *Int. J. Mol. Sci.*, **14**, 18284–18318.
 61. Morozko, E.L., Nishio, A., Ingham, N.J., Chandra, R., Fitzgerald, T., Martelletti, E., Borck, G., Wilson, E., Riordan, G.P., Wangemann, P. et al. (2015) *ILDR1* null mice, a model of human deafness *DFNB42*, show structural aberrations of trichocilia

- tight junctions and degeneration of auditory hair cells. *Hum. Mol. Genet.*, **24**, 609–624.
62. Jones, T.A., Jones, S.M., Vijayakumar, S., Brugeaud, A., Bothwell, M. and Chabbert, C. (2011) The adequate stimulus for mammalian linear vestibular evoked potentials (VsEPs). *Hear. Res.*, **280**, 133–140.
63. Petralia, R.S., Wang, Y.X., Hua, F., Yi, Z., Zhou, A., Ge, L., Stephenson, F.A. and Wenthold, R.J. (2010) Organization of NMDA receptors at extrasynaptic locations. *Neuroscience*, **167**, 68–87.
64. Sun, W., Maffie, J.K., Lin, L., Petralia, R.S., Rudy, B. and Hoffman, D.A. (2011) DPP6 establishes the A-type K(+) current gradient critical for the regulation of dendritic excitability in CA1 hippocampal neurons. *Neuron*, **71**, 1102–1115.
65. Johnson, G.A., Badea, A., Brandenburg, J., Cofer, G., Fubara, B., Liu, S. and Nissanov, J. (2010) Waxholm space: an image-based reference for coordinating mouse brain research. *Neuroimage*, **53**, 365–372.